Satellite Derived Bathymetry in the Canadian Archipelago Using Multi-spectral and LiDAR Space-based Remote Sensing

by

Natalie Ki Treadwell

A Thesis Presented to the
FACULTY OF THE USC DORNSIFE COLLEGE OF LETTERS, ARTS AND SCIENCES
University of Southern California
In Partial Fulfillment of the
Requirements for the Degree
MASTER OF SCIENCE
(GEOGRAPHIC INFORMATION SCIENCE AND TECHNOLOGY)

May 2022

Dedicated to my Father; thank you for instilling in me a lifelong love for the Arctic.

Table of Contents

List of Figures

List of Tables

Acknowledgements

I recognize that this study is conducted on Inuit and Inuvialuit coastline and adjacent seas. I acknowledge this thesis surveys the traditional land and seas of resident First Nations with the belief that greater subsurface modeling can improve marine safety and help maintain sustainable Arctic communities. The completion of this thesis is not without great support from my thesis committee and the greater hydrographic, remote sensing, and data science community. I am ever grateful for the advice, encouragement, and prior discoveries which have all made this work possible. I want to thank Dr. Larry Mayer, Director of the Center for Coastal and Ocean Mapping at the University of New Hampshire and a contributing cartographer to the International Bathymetric Chart of the Arctic Ocean for his suggestion to look at the dangerous lack of coastal bathymetric data along navigational routes in the Arctic. Dr. Zhong Ping Lee, professor of Optical Oceanography at the University of Massachusetts, assisted me greatly while I was learning about the various methods of satellite derived bathymetric mapping and for his introduction to Dr. Rodrigo Garcia, who was instrumental in the troubleshooting of NASA data analysis software, SeaDAS. I must also thank Dr. Chris Parrish, who developed the refraction correction which makes it possible to obtain bathymetry from ICESat-2 LiDAR photon returns. The support of Dr. Parrish helped me correctly reproduce his refraction correction and successfully navigate the challenge of ocean datum conversions. I would also like to extend my deepest gratitude to William Jacob McClure of Utah State University whose assistance in navigating the error codes of MATLAB was invaluable towards the completion of this project. Finally, I would like to thank my thesis committee members, Dr. Andrew Marx and Dr. Rodrigo Garcia for their support and feedback and my thesis advisor Dr. Fleming for his strong guidance throughout this whole process.

Abbreviations

ACOLITE	Atmospheric Correction for OLI 'lite', Royal Belgian Institute of Natural Sciences
ARCSI	Atmospheric and Radiometric Correction of Satellite Imagery
ATLAS	Advanced Topographic Laser Altimeter System
CHS	Canadian Hydrographic Service
DFO	Department of Fisheries and Oceans, Dominion of Canada
GEBCO	General Bathymetric Charts of the Oceans, International Hydrographic Organization
H_{Imager}	Satellite derived bathymetric depth
H_{LiDAR}	Depth from ICESat-2 data
IASC	The International Arctic Science Committee
ICESat-2	Ice, Cloud, and land Elevation Satellite
IHO	International Hydrography Organization
IMO	International Maritime Organization
IOC	Intergovernmental Oceanographic Commission of UNESCO
IOPs	Inherent Optical Properties
L2gen	Level-2 processing in NASA's SeaDAS program,
LaSRC	Landsat 8 Surface Reflectance Code
LiDAR	Light Detection and Ranging
MBVA	Multiband Value Algorithm
NONNA	Non-Navigational Bathymetric Data
NSB	Near-shore Bathymetry
NSIDC	United States National Snow and Ice Data Center
OLI	Operational Land Imager [Landsat 8 Constellation]

OSW	Optically Shallow Water
RMSE	Root Mean Square Error
R_{rs}	Remote Sensing Reflectance (Ocean color)
SDB	Satellite Derived Bathymetry
SeaDAS	Sea Data Analysis Software (NASA)
SONAR	Sound Navigation and Ranging
TBVA	Two Band Ratio Algorithm

Abstract

Just over 14% of the Canadian Arctic Ocean has been surveyed using multi-beam sonar mapping techniques, and comprehensive charting of navigable shallow water is even more scarce. With the use of LiDAR satellites and multispectral sensors, optically shallow water (OSW) that is free of sea ice can be modeled remotely through a process called Satellite Derived Bathymetry (SDB). Using two empirical algorithms, the multiband value algorithm (MBVA) and the two-band value algorithm (TBVA), bottom depth (H) in the Bellot Strait is interpolated. The study area is between 71˚ and 73˚ of latitude where North America meets the Somerset Island. Shallow water depth can be interpolated using LiDAR data which is collected by the ICESat-2 satellite, equipped with the Advanced Topographic Laser Altimeter System (ATLAS) that records ellipsoidal heights with uncertainties up to 0.70 m. The multispectral data is provided by the Landsat-8 Operational Land Imager (OLI) constellation at 30 m resolution. The MBVA and TBVA use refraction corrected LiDAR depths (H_{LiDAR}) within raster cells which overlap LiDAR returns to create a training dataset to inform interpolation of the SDB depth (H_{Imager}). SDB offers the ability to chart remote shallow places that would be difficult and expensive to reach otherwise. With the introduction of the Seabed 2030 project by the International Hydrography Organization (IHO) and the United Nations this past year, LiDAR refraction correction and SDB modeling has the potential to accelerate charting of coastlines, contributing towards our global pursuit to create stronger models of the Ocean seafloor and improve maritime safety. This thesis assesses the challenges of conducting SDB analysis in the Arctic region, using the Bellot Strait as a study area. Where appropriate remote sensing data exists, this process can be repeated.

Chapter 1 Introduction

In 2018, the Akademik Loffe, a passenger vessel traveling through the Northwest Passage, ran aground in the Gulf of Boothia. The grounding stranded 163 people and caused a discharge of about 20 gallons of fuel into the Arctic Ocean. The marine investigation report found the ship's captain made his navigation calculations using an incomplete bathymetric chart published by the Canadian government in 1998. (Transportation Safety Board of Canada 2021). Despite the grave environmental risks associated with loosing fuel or infrastructure overboard, lives can also be quickly at stake when considering hypothermic conditions, prolonged rescue and medical response time, and navigation conditions that drastically complicate disaster relief efforts. While the Akademik Loffe certainly is not the first vessel to face challenges in shallow polar waters, it is a reminder that Maritime activity is exponentially growing in a region where humankind still has not completed an accurate navigational charting. Figure 1 displays the 51 grounding that occurred in over 800 ship accidents recorded in the Artic Circle from 2005 to 2017, as compiled by the eight-nation Arctic Council working group, Protection of the Arctic Marine Environment. (PAME 2021).

The Arctic is known for its risks, especially for mariners; we have a greater topographic mapping of the Moon and of Mars than we do of the increasingly accessible Arctic Ocean. Bathymetry is the representation of depth underwater; this metric is vital to surface and subsurface navigation, seafloor geology, deep-water current and tidal modeling, and environmental monitoring. The main barrier to bathymetric mapping in polar regions is thick multi-year sea ice, which makes it impossible for ships with multibeam sonar to enter safely.

Submarine and other remotely operated submersibles can map under the sea ice; however, these methods are expensive and limited in their scope.

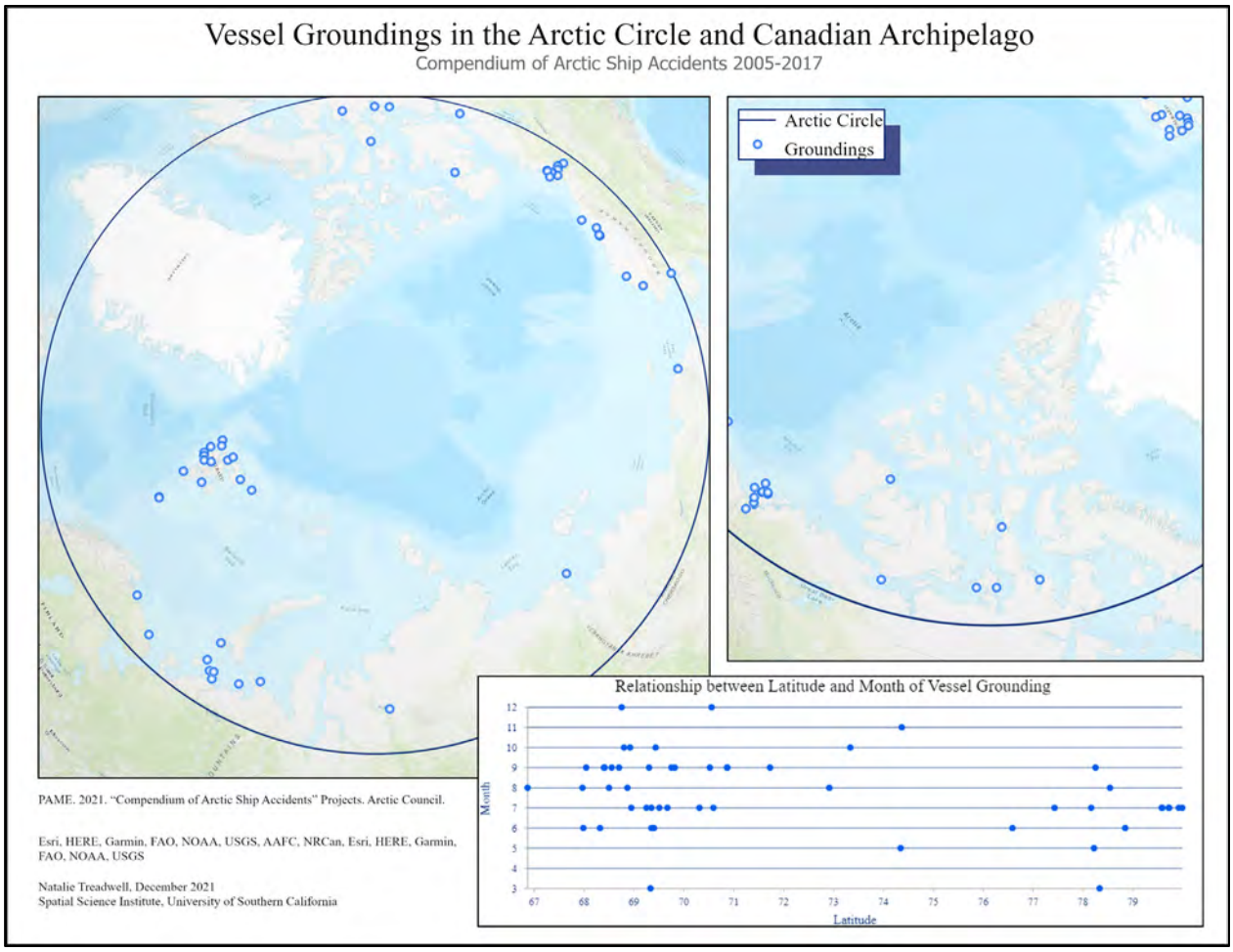

Figure 1: Ship Groundings from 2005 - 2017 (PAME 2021)

Another barrier to modeling the Arctic seafloor is the inability for icebreakers or submersibles to reach shallow waters, leading to a general lack of nearshore data regardless of how often that area is navigated or surveyed. A common alternative to shipborne remote sensors is light detection and ranging (LiDAR) equipped flights that can generate bathymetry of coastlines containing optically shallow water (OSW). It is important to note that industry standard polar datasets are typically expensive to procure and data collection at the poles face

many technical, financial, environmental, and logistical challenges. Flights utilizing LiDAR are expensive, requiring significant planning and good weather, making the Arctic region one of the most difficult places on earth to coordinate active or passive data extraction via airplane. This thesis conducted an alternative method of mapping depth in shallow Arctic regions using training data derived from satellite LiDAR; Satellite Derived Bathymetry (SDB) is a type of spatial analysis which uses space-borne LiDAR and multibeam satellite imagery to interpolate depth up to 30 meters below sea level. The spatial analysis relies on the reflectance of light in shallow water as a function of depth and other optical and bottom properties, proved first in the 1980's by Dr. Lyzenga, a University of Michigan researcher. (Lyzenga 1981) Over the past thirty decades, improvements to these methods have been made expanding the potential for remote bathymetry interpolation using satellite remote sensing, most notably the work done by Dr. Parrish through the University of Oregon to account for the change in LiDAR laser speed between air and water which is not corrected for in the raw data provided by the National Snow and Ice Data Center (NSIDC). (Parrish 2019) Few SDB experiments have been conducted in the Arctic as this method of spatial analysis is typically used in more clear, tropical waters. Considering the difficulty of airborne LiDAR flights in the Arctic, SDB is an apt method of conducting shallow water depth interpolation. This thesis will explore SDB methodology to interpolate depth of OSW in the Bellot Strait, a route commonly used in navigating the Northwest Passage through the Arctic Ocean.

This thesis argues that a SDB map of the Bellot Strait can be accomplished with reasonable statistical certainty using ICESat-2 and Landsat-8 OLI imagery and similar methods could be utilized to map regions with comparable data across the Canadian Archipelago. The work of this thesis pulls together recommendations from several SDB studies to create a

MATLAB based code that can be further utilized with datasets collected over alternate study areas. While other forms of multispectral or LiDAR data collection could be used to accomplish a similar model, the conclusions of this body of work only address ICESat-2 and Landsat-8 Operational Land Imager (OLI) Collection 1 Level 1 30 m resolution data. Nearshore bathymetric modeling goals can be achieved through many types of remote sensing tools; the work presented in this thesis only uses open-source datasets, software, and geospatial tools with the intentions of creating a methodology which retains open-source accessibility. There are still great opportunities to explore the nuance between alternative SDB data sources and geospatial correction methods. Further study on the use of alternative forms of LiDAR and higher resolution multispectral imagery to produce SDB in the Arctic is required. The results of this thesis should be understood as a unique byproduct of the ICESat-2 and Landsat-8 satellite systems.

A 2017 study into the navigable routes of the Northwest Passage reveal that a route which includes the Bellot Strait is considered the best navigable expectation when considering ice events in the Northwest passage. The study referenced a survey conducted from 2006 – 2015, which noted that the Bellot Strait is open and navigable to boats with a hull depth of 10 m as early as July 21st and closes as late as October 19th. (Liu et al. 2017) The Bellot Strait connects the Gulf of Boothia with the Peel Sound, between the Somerset Islands and the Boothia Peninsula, located in the Nunavut Territories of Canada. The study area includes three distinct bays with swift currents surrounding shallow regions and a series of islands near either entrance to the strait.

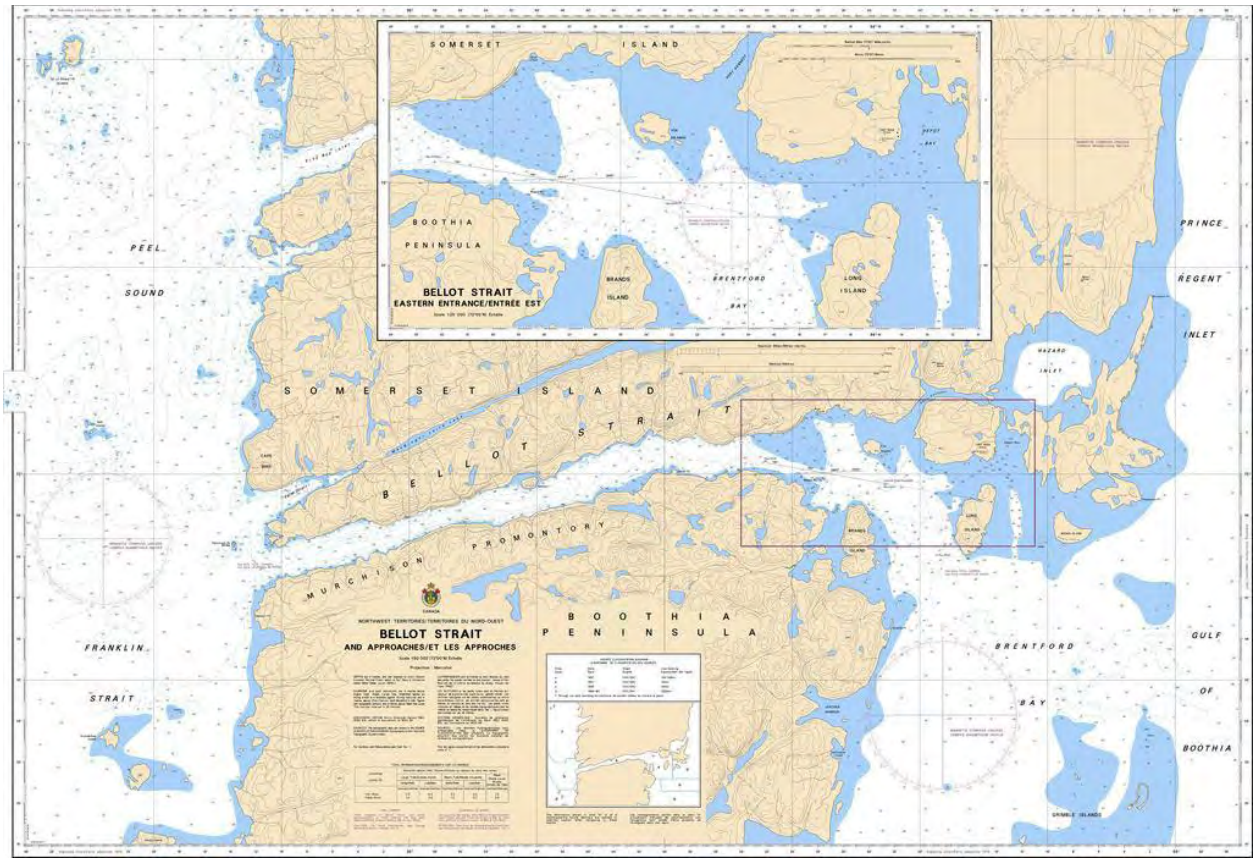

Figure 2: Canadian Nautical Chart of the Bellot Strait, Nunavut (CHS 2020)

Figure 2 depicts the Canadian Nautical Chart published in 2020 of the regions surrounding the Bellot Strait, however the raw data from the chart is not available for digital public access. The Canadian Hydrographical Survey (CHS) however released non-navigational (NONNA) bathymetric data, which was used to predict where the SDB models might be successful. Figure 3 reveals the deepest section of the Strait is approximately 404 meters deep and shows that the area to the East of the Strait, Hazard Inlet, has not been comprehensively mapped. Areas in red, orange, and yellow are expected to be under 20 meters and represent

OSW. From the NONNA data, it is predicted that optically shallow water will be found near inlets and alcoves, specifically Hazard Inlet.

SDB charting in the Arctic Ocean has the potential to increase our ability to navigate and monitor change in these regions. More accurate charts of near-coastal water are relevant to mariners who might need to navigate shallow waters, to hull insurers who charge a premium for ships using the Arctic Ocean, and to various government agencies and international organizations charged with charting the oceans and developing best practices for Arctic shipping.

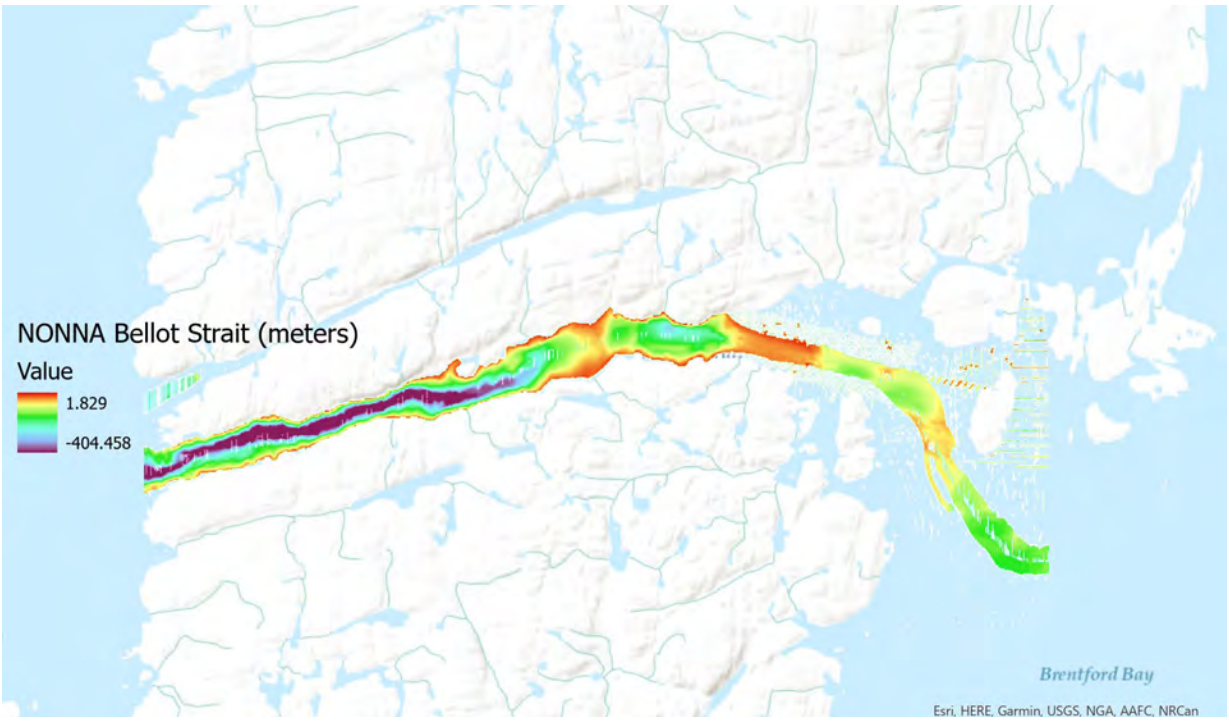

Figure 3: NONNA bathymetry of the Bellot Strait

Government agencies include but are not limited to the Arctic Councill, the National Oceanic and Atmospheric Association (NOAA), the Canadian equivalents, Department of Fisheries and Oceans (DFO), and the Canadian Hydrographic Association (CHS) as well as the International Maritime Organization (IMO). While these groups might be interested in process

and conclusion of this thesis, IMO and CHS standards for nautical charts are strict and have not been expanded to adopt data from Satellite Derived Bathymetry. (Kutser et al. 2020)

The Arctic is a complex region governed by the eight Arctic coastal or land states who have claim to the internal waters, territorial seas, exclusive economic zones, and land that surround the international waters of the Arctic Ocean. These nations are the United States, Canada, Denmark for Greenland and the Faroes, Iceland, Finland, Sweden, Norway, and Russia; all whose territory lies above the Arctic Circle at 66°33' N. Maritime and Jurisdiction boundaries of the Arctic Nations is detailed in Appendix A, compiled in a map published by the Durham University geography department. Conflicting sovereignty claims have been filed in the Arctic and with annual decline in sea ice, this region will continue to be a stage for geopolitical discourse. There are several regional, government, and intergovernmental groups whose work is dependent and highly affected by the bathymetry of this region.

PAME / Arctic Council

The Arctic Council is an intergovernmental forum that works with Arctic states and observing nations to promote the cooperation and coordination of activities North of 60°. The group develops working committees who address issues from emergency response to environmental monitoring and sustainable development. The Protection of the Arctic Marine Environment (PAME) committee works to collect Arctic Ocean data, monitor maritime activity, and advocate for fair development of trade routes. PAME released the Compendium of Arctic Ship Accidents, which provided the data used in Figure 1 to highlight groundings that have occurred between 2005-2017. The dataset records ship accidents in the Arctic Ocean, containing coordinates for everything from sinkings, passenger fatalities, partial groundings, and total bottom contact. Ship

accident records inform the need for greater bathymetric survey, improve emergency response times, and contribute significantly towards mapping navigational dangers and improving ship design.

International Hydrography Organization

The International Hydrography Organization (IHO) is another intergovernmental group that monitors and promotes the surveying and charting of seas, oceans, and navigable waters. The group works to create uniformity between nautical charts and maritime regulations in Member States. The IHO is the predominant worldwide hydrographic organization, their regulations help maintain consistency in the bathymetric process. The International Bathymetric Chart of the Arctic Ocean initiative to develop a uniform database of all available bathymetric data north of 64˚ of latitude is sponsored by the IHO to produce a robust interpolation of the seafloor of the Arctic Ocean.

International Arctic Science Committee

The International Arctic Science Committee (IASC), founded in 1990, is a council focused on strategic action groups, working groups, and implementation of science development support. Their five working groups composed of two scientists from each of the 23 member states to address Terrestrial, Marine, Atmosphere, Cryosphere, and Social & Human to provide strategic recommendations for Arctic management plans. IASC is also a contributing member to the global volunteer initiative to create an International Bathymetric Chart of the Arctic Ocean.

Intergovernmental Oceanographic Commission

The United Nations working group responsible for furthering ocean science and services is the Intergovernmental Oceanographic Commission of UNESCO (IOC). The group works to support 150 Member States to work together in pursuit of UN Agenda 2030 as well as other sustainable development goals. Their main objective is to manage and protect oceans, coastline, and marine ecosystems worldwide. The IOC sponsors several bathymetric projects in the Arctic Ocean and their focus on mapping the Arctic Ocean is part of the Seabed 2030 project. Under the IOC is the Arctic Regional Hydrographic Commission, which operates through the IOC's working group focused on the Arctic.

NOAA

The National Oceanic and Atmospheric Administration is a US Government organization responsible for monitoring ecosystems for everything from daily weather forecasts to real-time disaster management, and environmental monitoring. NOAA certifies and publishes all the nautical charts along US coastline through the Office of Coast Survey. NOAA uses SDB to monitor areas that are constantly changing and help determine where new multi-beam or airborne LiDAR surveys should occur. NOAA has recently contracted a private company, TCarta, to produce bathymetry using the Maxar satellites and the radiative transfer method along the coast of Alaska to help inform future surveys. It seems that this technique is valuable towards identifying lack of information or discrepancies in charts, however NOAA does not currently publish charts with data from SDB methods.

Canadian Hydrographic Survey

The Canadian Hydrographic Survey (CHS) is a division of Fisheries and Oceans Canada (DFO) which funds and publishes surveys, navigational products, and nautical charts. Their website offers free 10 m and 100 m resolution charts of the Eastern Beaufort Sea to Baffin Bay, as well as areas southbound of Baffin Bay above 60° N. CHS is working in conjunction with the Canadian Space Agency to implement SDB to fill gaps in remote shallow Canadian waters. Their methods use band ratio and multi-band approach which both rely on previously surveys for training data, limiting their ability to use the methods in areas that have never been surveyed. While the study outlining the CHS's use of SDB was published in 2018, it is unclear from their website or other publications how intensely they rely on SDB. (Chéneir et al. 2018)

Further examination of the history of mapping in the Arctic, the SDB process, and applications of this method above the Arctic Circle will be explored in Chapter 2, the related works section. Chapter 3 explains the specific SDB process used as well as a comprehensive review of the data and satellites that make this spatial analysis possible. Chapters 4 through 6 address the results of the SDB method and discuss the applicability of ICESat-2 derived SDB within the Canadian Archipelago.

Chapter 2 Related Work

2.1. History of Arctic Bathymetry

The Arctic Ocean is one of the least navigable and scarcely charted bodies of water on Earth. Sailing through its waters has been a nautical holy grail (at least for European sailors) since the 1500's, and for Vikings long before that. For the greater majority of recorded human history, the geographic representation of the Arctic has been either completely postulated or pieced together using interpolation and assumption. Geographers - up until the last ten years of the nineteenth century - believed that the North Pole consisted of land covered in snow or a series of archipelagos. (Weber 1983) The development of ships that could withstand Arctic waters allowed for lead line survey, which was the predominant method of calculating bathymetry until mid-20th century; ropes or lines with depth markings and lead weights were manually lowered at positions determined with a three-point sextant affixed to nautical chart reference points. The first ship to survey the Arctic with this method was the *Fram*, a Norwegian ship designed and captained by Fridtjof Nansen to drift with the ice and push the hull upwards so that it would sit atop the sea ice. The *Fram* traveled between 1893 and 1896 drifting to a latitude of 85°14' N, failing to reach its goal of drifting towards the North Pole, stopping just short of Svalbard. The expedition found the Arctic Ocean was not a series of islands but rather a deep basin extending at least 3000 m deep, leading geographers to initially represent it as one singular basin. It was not until a tidal analysis conducted in 1904 by a U.S. Coast and Geodetic Survey that officer Rollin Harris hypothesized a divided barrier or ridge as the flow of ice alluded to two different periods of tidal oscillation within each basin. (Levere 1988) Lead line surveys continued well into the 20th century, slowing during WWII, and later supplemented by Soviet military aircraft that would land on the ice to conduct soundings using an explosive charge and a

stopwatch. The Soviets led 87 surveys across the Arctic Ocean from 1948 to 1950 revealing the ridge separating the two basins through soundings retuning shallow depths of 1290 m. Soviet records led to the discovery of the underwater mountain range that extends from the New Siberian Islands to Ellesmere Island. This mountain range was named after an 18th century geologist Mikhail Lomonosov and is commonly referred to as the Lomonosov Ridge. (Weber 1983) The discovery of the subsurface ridgeline changed the modern conception of the northernmost ocean and jumpstarted a race to map the seabed of the Arctic.

Both world wars, the following Cold War, and widespread US, Russian, and British use of submarines in the Arctic, led to the development and commercialization of Sound Navigation and Ranging (Sonar) throughout the 20th century. Sonar works using a system called a transducer, which is a physical sound sensor that emits an acoustic pulse and absorbs the sound waves that return using a device called an array. Sound waves are successful in this application because they travel further than light or radio waves would. Active sonar emits a pulse to measure distance, range, and orientation using a signal emitted by the system while passive sonar detects noises from object or creatures generating sound in the water. Single beam sonar uses one transducer to emit and receive acoustic energy while multibeam emits several signals to cover a larger study area. These methods of survey are commonly installed on large ships for navigation and creation of nautical charts. (NOAA 2021) Sonar revolutionized the ability to map large areas of deep and shallow water, however it is more difficult in remote and hazardous Arctic waters where icebreakers and other ships are incapable of entering shallow water. Despite the challenges of using this process in shallow water, the development of sonar mapping products in the past century have so dramatically increased portrayal of the seafloor that all previous maps should be considered obsolete. (Jakobsson et al. 2014)

Another important method of remote bathymetric sensing developed in the 20th century is the use of a laser pulse altimeter to measure distance from the sensor to the nearest object. This process is called Light Detection and Ranging or LiDAR and is accomplished by calculating the time it takes for a pulse of green wavelength laser light to return to the sensor. LiDAR monitoring changed the ability to map features both above and below sea level and the application, use, and study of LiDAR from the 1950's through the 1970's led to its use in bathymetric survey. The first bathymetric LiDAR survey was conducted in 1968 in the Atlantic Ocean, but it was not until 1985 that the CHS first mapped the Arctic with LiDAR. The Optech Larsen-500, an early commercial airborne LiDAR, used a green wavelength laser to penetrate up to 50 meters where Arctic water was clear and shallow enough. In 1988, the CHS released their first chart using LiDAR and have since continued to incorporate airborne sensing as it proved to be safer, quicker, and more efficient than the predominant method of single and multi-beam sonar readings. (Ackerman 2017) This technology continued to improve and was first tested using satellites with the launch of the Ice, Cloud, and Land elevation Satellite (ICESat) in 2003 as a part of NASA's Earth Observation System. LiDAR systems have contributed significantly to elevation and optically shallow water calculations improving the accuracy of our remote sensing to errors as low as 70cm. The first ICESat satellite conducted laser altimetry readings from 2004-2009 but it was not until the launch of the ICESat-2 Advanced Topographic Laser Altimetry System in 2018 that bathymetric photon returns were detected. Spaceborne LiDAR SDB is still a relatively new process and datasets from these satellites have yet to be tested to their full potential. (NSIDC 2021)

The Arctic, as we understand it in the 21st century, is one of the last remaining frontiers; we are still working to chart, model, and understand the geography, climate, and biodiversity of

the North. International groups, Arctic Nations, and scientific organizations have been developed to address the rapid ecological, cultural, and policy change occurring in the Arctic. One common objective among these groups is to chart the entirety of the Arctic Ocean.

2.1.1 International Bathymetric Chart of the Arctic Ocean

The most comprehensive chart of the Arctic Ocean currently available is the International Bathymetric Map of the Arctic Ocean (IBCAO) version 4.0, released in 2020, with a resolution of 200 m x 200 m on a polar stereographic projection. IBCAO is a joint project between the IHO, IOC, IASC, Arctic coastal and land states, as well as affiliation from 24 institutions in 10 countries[1]. These volunteer efforts have compiled data from multi-beam and single beam sonar research vessels, shipping, and fishing vessels (running a commercial sonar system called the Olex seabed mapping software), and military submarines. The project originated in 1997 to build upon the CHS General Bathymetric Chart of the Oceans (GEBCO), which contained little data for the Arctic basin. At the time of GEBCO's drafting, icebreakers had not conducted sounding research very far into the ice pack. (Jakobsson et al. 2014) As of 2021, only 19.8% of the Arctic Ocean has been surveyed using single or multi-beam sonar as referenced to the Seabed 2030 model. Depth estimations for grid cells between observations were interpolated using a continuous curvature spline with a tension gridding algorithm. Lack of data in nearshore areas has resulted in a poorly constrained spline function, or NSB data used in IBCAO is based on incomplete nautical charts, resulting in the difficulty of calculating error in shallow areas. To contribute towards the reliability of the IBCAO, a maximum and a minimum depth grid have

[1] Canada, Denmark, Germany, Iceland, Italy, Norway, Russia, Spain, Sweden, USA. (NOAA/NCEI & World Data Service for Geophysics. 2012.)

been published respectively as the bathymetric model is limited by its underlying data. (Jakobsson et al. 2020). The IBCAO has recently merged efforts with The Nippon Foundation, a philanthropic organization that promotes marine and shipping activities, and the GEBCO to map the global seafloor by 2030. This merger occurred at the 2019 Fall Meeting of the American Geophysical Union in when version 4.0 of IBCAO was released under the auspices of the Nippon Foundation-GEBCO-Seabed 2030 Project. (Jakobsson and Mayer 2019)

2.1.2 Arctic Ocean Mega Project

The Arctic Ocean Mega Project is another noteworthy survey of the Arctic Ocean seafloor addressing the geology, bathymetry, seismic lines, magnetic anomalies, continental shelves, and geodynamics which contribute to the evolution of the Arctic Ocean. This project is spearheaded by the Russian Government and is an evolution of their 1950's aerial-based surveys. While this study focused primarily on deep water in the Arctic Basin, it addresses the geology of the Northwest Passage, which is relevant to my study. As of 2021, the project is the largest comprehensive benthic database of the Arctic that has been created using nuclear icebreakers and submarines.

2.1.3 Arctic Net

The Arctic Net Program, sponsored by the Canadian Government, works to understand, and mitigate the impact of climate change on the Canadian coast. Their objectives span from developing knowledge in the Arctic, preserving local language and history, and devises a science-based approach to conserving the Arctic. Arctic Net sponsors the Arctic Mapping Program, a campaign to collect backscatter and sub-bottom data in the Canadian Arctic.

2.2. Shallow Water Bathymetry and Satellite Derived Bathymetry

Optically shallow water (OSW) are locations where light reflected off the seafloor contributes to the water-leaving radiance, or bottom reflected light. The amount of bottom reflected light is directly proportional to the optical depth, which is assigned through a combination of the waters inherent optical properties (IOPs) and depth. (Lee et al. 1999; McKinna and Werdell 2018) This phenomenon is usually observable up to a depth of 20 meters, however, in more turbid waters, a depth of only 3 meters or less might be observable. (Kutser et al. 2020; Coveney et al. 2020)

Analysis of OSW has been greatly aided by the introduction of multispectral satellite sensors in the ‘70s through the launch of Landsat and other multispectral satellites. (Smith et al., 1975; Jupp, et al. 1985) Space-based imagers allowed for greater monitoring of coastal regions through repetitive multispectral imagery, allowing researchers to compare coastlines over time and obtain reliable change monitoring of water properties. (Olmanson et al. 2008; Knudby et al. 2010) SDB techniques were heavily developed in the ’80s and ‘90s to monitor coral reefs and coastal erosion, and most of the published studies from that era focus on clear tropical ocean water, or freshwater lakes and streams. (Bour et al. 1986; Mumby et al. 1994; Kutser et al. 2020)

David Lyzenga, a researcher at the University of Michigan, demonstrated that bathymetric interpolations could be calculated using depths acquired from LiDAR surveys that are collocated to remote sensing reflectance data (R_{rs}) from a multi-spectral. His 1985 paper proved that the relationship between depth and reflectance can be represented as an estimation for each raster cell. The initial experiment was performed in two test sites in the Bahama Islands (North Cat Cay and Bimini Bay) and the results found calculated root mean square error and observed root mean square error of less than one meter. (Lyzenga 1985) Further improvements

on this method have been used to characterize coastal environments and map the structure of habitat canopies, monitor erosion, tidal change, and model reflectance of bottom substrata. As these methods were improved upon throughout the end of the century, the relationship between depth and reflectance became better understood as exponential, rather than linear. The potential error of depth eventually reaches a point where the depth of reflectance penetration no longer changes with the depth of the water. This point is when the water is no longer optically shallow, usually around 20-30 meters depending on the water turbidity and sedimentation present in the water. (Kutser et al. 2020) While these methods have been successfully applied in tropical equatorial waters, the weather, glacial sedimentation, and turbidity in the Arctic drastically complicate this process.

Active sensor bathymetric surveys using hydrographic survey tools include multi and single beam sonar, remotely operated vehicles (ROV), AUV fitted with LiDAR, or the lead line method. (Kutser et al. 2020) These forms of remote sensing are expensive, limited to areas that are accessible to surveyors, and without routine surveying, produce data with poor temporal resolution. Space-borne LiDAR allows for repetitive global monitoring of earth terrain and weather patterns, helping to procure digital elevation models, map tree canopy, and in some instances can be used to model near shore bathymetry. The ICESat (launched in 2003) and the ICESat-2 (launched in 2018) have procured granular LiDAR data with errors as small as 70cm. While the development of these satellite systems was focused mainly on mapping terrain above sea level, its improvements vastly changed our use of aerial remote sensing of optically shallow water. The development of LiDAR based bathymetric models in the 80’s led to the ability to calculate depths using space-based remote sensing once the satellite data became available.

2.3. SDB in the Arctic

There are only a few studies conducting SDB within the Arctic region; considering the scarcity of clear multispectral images, lack of multibeam sonar in shallow water, cost of airborne LiDAR, and emerging reliability from space-based LiDAR, the data has not always been available. The nature of this region makes it difficult to conduct any method of survey, let alone have a stable temporal resolution for near-shore bathymetry (NSB) as sea ice freezes to the shoreline for up to 10 months a year. Furthermore, ice scour or thawing of benthic ice beneath the ocean floor can also change underlying bathymetry. Other obstacles to obtaining imagery suitable for SDB are cloud coverage, floating ice, glacier powder, and rough coastal tides that often change throughout the season. In 2018, the Canadian Hydrographic Service (CHS) conducted a survey of three empirical SDB techniques to model NSB in Cambridge Bay, Nunavut. Their goal was to analyze the advantages and disadvantages of applying SDB algorithms to multispectral images available in the Canadian Arctic. The four satellite images were garnered from Worldview-2, Pléiades, SPOT, and PlanetScope between 2015 and 2017. The reference bathymetry comes from early airborne LiDAR flights from 1985 and 1992 as well as multibeam surveys conducted by ship from 2014-2017. The three approaches, which were determined to yield relatively the same error, are as follows:

Multi-Band approach - Identifies the depth at which visibility to the seafloor is not possible within each band used, then an empirical relationship is established between the reflectance of each band to calculate depth. This method, originally proposed by Lyzenga et al. (1985) and further refined by Lee et al. (2021) shows that leveraging multiple bands can help increase accuracy.

Band Ratio technique – Operates by quantifying the degree at which water absorbs various wavelengths of light between the green and blue bands. This method assumes that green wavelengths will penetrate deeper than blue wavelengths, meaning that the greater the difference in propagation between the bands results in the assumption of deeper water. This method was first pioneered by Stumpf et al. (2003) and has been referred to as the Two Band Ratio Algorithm (TBRA) by Lee et al. (2021). This empirical approach is good for areas that contain vegetation that might make the reflectance appear negative in some bands as this difference becomes more apparent when comparing the blue and green bands.

Multi-dimensional Look-Up-Table (LUT) –

This method works by taking known depth points and classifying them through a combination of bands which represent the pixel at a known depth. The range of band values are assigned to a depth, which creates a Look-Up-Table (LUT) that can be applied to the Satellite imagery using Euclidean distance algorithms. For each of these three approaches, an object-based image segmentation was applied using eCognition to create polygons around all areas in the image that seafloor is visible to filter which parts of the image are used in the assessment. (Aloha et al. 2018)

In 2019, a group of researchers working through the First Institute of Oceanography under the Chinese Ministry of Natural Resources used the AI statistical model Support Vector Regression (SVR) and inverse distance weighting interpolation to create a SDB map in the Russian Arctic. Their study area focused on the southside of Kolguyey island, an inlet in Northwest Russia where the 100 km strait, Pomorskiy Proliv, connects the Barents Sea to the

Pechora Sea. Researchers leveraged chart data surveyed using shipborne sonar and Sentinel 2 multispectral imagery. From the soundings, 201 points were selected evenly amongst four depth intervals from 0-20 m, with 0.3 m of additional height added uniformly to simulate depth in accordance with the tides. Sentinel 2 data was then processed through the European Space Agency, Sen2cor program, to apply bottom-of-atmosphere reflection correction and other relevant land and atmospheric masking. SVR was implemented using the preprocessed sonar and multispectral data to generate collocated R_{rs} and depth. The selected chart points were then used to interpolate depth through ordinary kriging, pan kriging interpolation, inverse distance weighting, and spline function across uniformly distributed depth points. After comparing the root mean square error (RMSE) and mean absolute error (MAE), inverse distance weighting was determined to be the best fit interpolation within the study area. (Zhang et al. 2019)

2.4. Guiding Studies

The main study which makes the methods of this thesis possible is a refraction correction developed in 2019 that accounts for the refraction at the air/water interface as the change in the speed of light which occurs when the photon penetrates the water. (Parrish et al. 2019) This correction algorithm uses geometry to account for the change in laser photon speed that occurs at the air water interface. The ATL03 data product provided by the NSIDC is processed through an algorithm which calculates height above the ellipsoid dependent on surface type, at this time there is not a dataset available through the NSIDC where refraction correction is applied to bathymetric points. Without refraction correction, the ATL03 points showing land height are both off nadir and deeper than reality. (Parrish et al. 2019) The algorithm accounts for both vertical and horizontal offsets and ends up making slight corrections to latitude, longitude, and

height. The variables needed for the refraction correction are extracted using available ICESat-2 ATL03 data from the NSIDC in HDF5 format. Parrish and his team developed eleven algorithms which perform the refraction correction. The equations detailed within the method section of this thesis are adapted from his study and reformatted to include calculations described by Parrish for clarity of the MATLAB code. The correction of ATL03 photon returns has been successfully applied across several study areas worldwide since Parrish proved the refraction correction. However, since this method has been published, it has only been applied to Arctic waters once. (Ranndal et al. 2021)

Published in August of 2021, researchers at the University of Denmark used ICESat-2 to evaluate the process of applying refraction correction to calculate bathymetric photon returns from ATL03 data over Greenland. (Ranndal et al. 2021). The algorithm outlined in Ranndal is modeled off the correction algorithm created by Parrish et al. (2019) and applies the correction to data taken over the central West coast of Greenland, around Sisimiut. Results showed that ICESat-2 bathymetric returns exhibited a high amount of noise and that the majority of bottom sites were too deep for LiDAR collection. After filtering the ATL03 refraction corrected data to remove points labeled by researchers, only a small amount of photon return data could be labeled as bathymetry. The study concluded that under strong enough quality constraints and supervision from researchers, the approach created by Parrish can be validated for obtaining bathymetry locally using LiDAR. However, the researchers cautioned upon using this method in areas where bathymetry is not known and argued that a deep learning approach targeting different water systems and informed by known bathymetry could better leverage the data provided by ICESat-2 to map remote shallow areas.

The method of this thesis primarily follows a study published in April of 2021 by the University of Massachusetts, Boston which presents a prototype method for SDB which fuses LiDAR data and multiband imagery to create a SDB map using the multiband value algorithm. Lee et al. (2021) overcomes the main challenge posed by other SDB methods through bypassing the need for training data from sonar or other NSB surveys by instead leveraging Parrish's 2019 refraction correction of satellite LiDAR. The process uses data from ICESat-2, which is a single-photon-sensitive detection technique that provides vertical resolution with accuracy up to 0.70 m in OSW. Lee and his team looked at several empirical and semi-analytical methods of producing SDB using space-based LiDAR and multispectral imagery and showed that the Two-band value algorithm and the Multiband Value Algorithm returns are location and data dependent but can return reliable bathymetry.

Another study that helped guide development of the methods leverages the two-band value algorithm to produce a bathymetric DEM from the combination of IceSat-2 and Sentinel-2 or Landsat 8 OLI multispectral imagery. The geophysical research letter published in February of 2021 by the American Geophysical Union details the findings of a thesis produced by Benjamin Babbel at Oregon State University. Benjamin's thesis advisor for the project, (and co-author of the research letter) is Christopher Parrish. The work follows the refraction correction of Parrish and the ratio of logs algorithm put forward by Stumpf to create a SDB map using ground point validation from ICESat-2 data over the U.S. Virgin Islands, specifically the island of St. Croix. Babbel writes that 'the highest priority for furthering automation [of SDB maps] support the long-range goal of global coral reef habitat change analysis using ICESat-2 and shows that the reliability of this model depends on its ability to be further tested in waters with varying bottom substrate, turbidity, light conditions, and bathymetric relief. Babbel outlines that this method

works well enough, (returning RMSE of 0.96 m for Sentinel-2 imagery and 1.54 m for Landsat 8), however site-specific characteristics greatly affect the error margins of this process. (Babbel et al. 2021) Due to the lack of near shore surveys in the Arctic, harsh environmental conditions, and short window of positive data return, the study area chosen for this thesis challenges the algorithms proven by these previous studies and strives to identify the variables which can make or break this process. If this model can be successfully applied in some of the world's most harsh and unforgiving climates, it could expand from being a tool primarily used to monitor coral habitats to instead help map the shallow inaccessible regions of the world.

Chapter 3 Methods

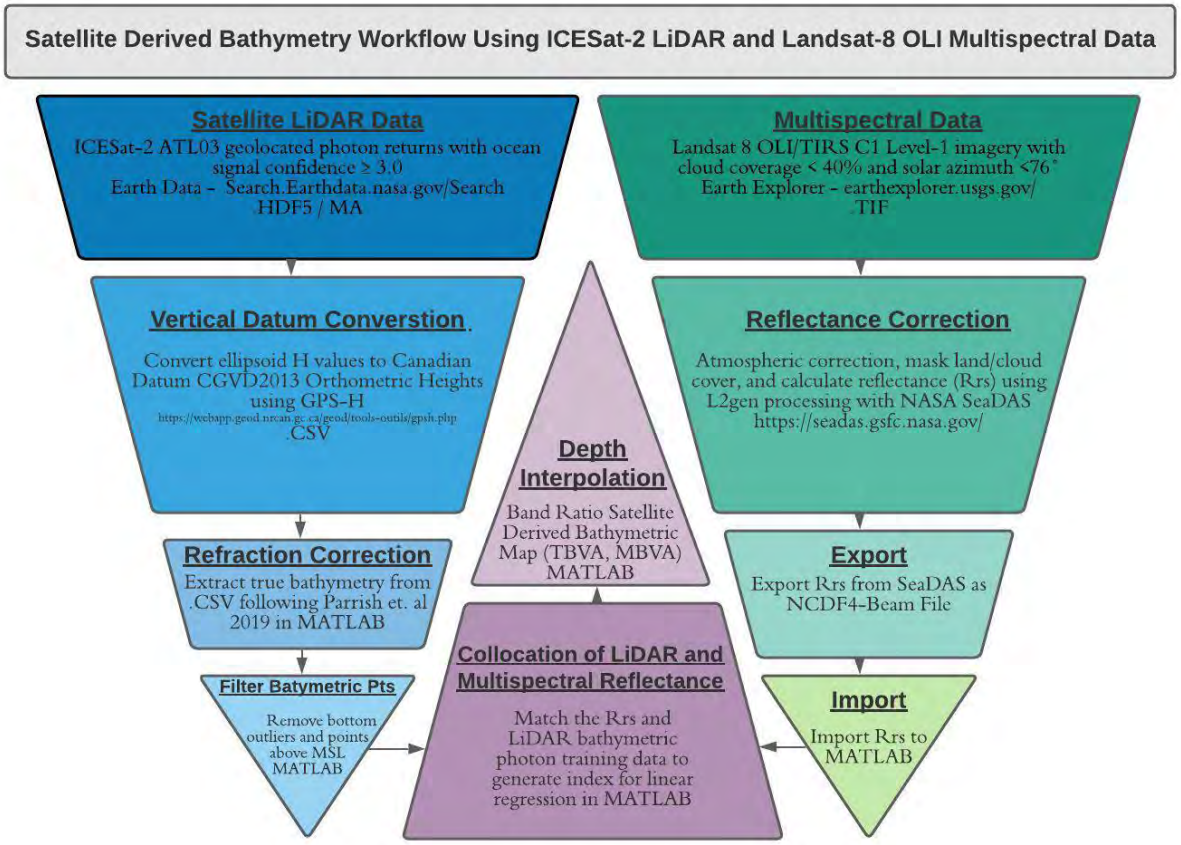

Figure 4: SDB Data Processing Workflow

The methods utilized in this thesis consist of unique preprocessing steps based on the location of the study area for both the multispectral and the ICESat-2 LiDAR datasets. While many forms of multispectral data could be applied successfully with these methods, Landsat 8 Collection 1 Level 1 data is utilized as the multispectral data source. Other satellite derived bathymetric processes address the use of airborne LiDAR or utilize other forms of seed ground truth data such as single-beam and multibeam sonar, or lead line techniques; the workflows addressed in this thesis are specifically designed to leverage the space-based LiDAR remote sensing available through the ICESat-2 mission. Figure 4 details the data processing workflow

from data download to depth interpolation including program and data citations, file type, and objective of the workflow step.

3.1. Data Acquisition

The primary threshold on data acquisition within the study area is open water conditions in the Arctic. In 2010, the Arctic Resources & Transportation Information System, an online database of resources regarding transportation, resource extraction, and logistic solutions compiled by the Centre for High North Logistics at Nord University in Northern Norway conducted a survey of sea ice density in Arctic shipping lanes. Their findings stated that the Bellot Strait is usually navigable and free of sea ice from late-August to late September, however these dates fluctuate depending on the average temperature for the season. (Liu et al. 2017) To ensure that signal interference due to sea and land ice was minimized, the ICESat-2 database search was limited to the months of August and September for 2019-2020. The satellite was launched in October of 2018 and data was sourced for this thesis in July of 2021, confining the available datasets to the temporal resolution of the ICESat-2 satellite: October 2018 – July 2021. Using the Open Altimetry portal created by the National Snow and Ice Data Center (NSIDC) and the National Aeronautics and Space Administration (NASA), datasets from the ICESat-2 satellite were explored for bathymetric photon returns. There are several data products available from the ICESat-2 photon returns; the NSIDC preprocesses photon return data to prioritize different parameters such as sea ice elevation, terrain elevation, LiDAR backscatter, canopy height, glacial and ice sheet elevation and more. For the purposes of extracting bathymetric photon returns, the ATLO3 terrain elevation dataset contains the necessary LiDAR to influence a SDB map. A survey into the ground tracks with available bathymetric photon return was conducted and results are highlighted in the discussion chapter of this thesis. Since the search for positive data returns

is to assess potential of future study areas, the methods section will not address the Open Altimetry survey. The review of available bathymetric datasets in the Canadian Archipelago was conducted after SDB data processing outlined in Method as it was considered an assessment of future work.

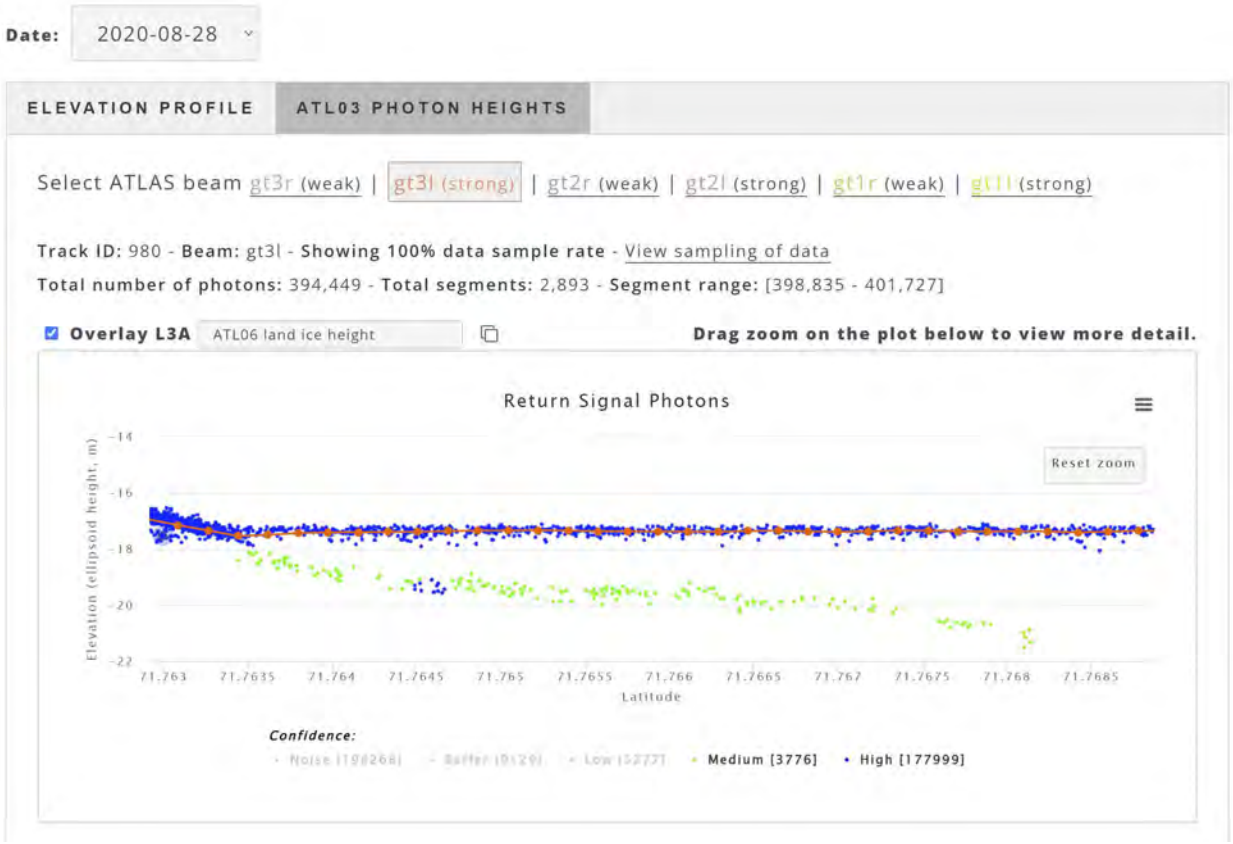

Figure 5: Open Altimetry data portal showing ATL03 data with bathymetric photon returns

ATLO3 data products are global geolocated photon height readings returning precise geographic coordinates (Latitude/Longitude in WGS-84), elevation, determination of signal or background photon, and classification of surface type as land ice, sea ice, land, or ocean. (NSIDC 2021) This data product returns six data points every 0.7 meters, or granules that are segmented to span 1/14th of an orbit. (Lee et al. 2021) The data is broken into six ground tracks, three containing strong returns and three with returns labeled weak. Using the ‘view elevation

profile' tool in Open Altimetry, land-ice height can be overlayed on return signal photons to identify areas where medium and high confidence photon returns have captured bathymetry. After searching through the five tracks which fly over the Bellot Strait, 9 datasets were found to be surveyed in August or September. Of those flyovers, only one dataset captured bathymetry, on August 28th, 2020, shown in Figure 5 where the land and water surface model is shown in orange (ATL04 Land/Ice height dataset) and subsequent bathymetric returns are found below the water surface model represented by points categorized as confidence three and four.

After identifying the ICESat-2 dataset, constraints were set on the Landsat-8 OLI dataset to 32 days on either side of the August 28 LiDAR collection date. The constraint is based on the 16-day repeat cycle of the Landsat-8 satellite allowing for the satellite to capture at least two images over the same area, increasing the likelihood that ice and cloud free imagery will be captured. Ice-free water tends to produce more evaporation which further complicates clear data acquisition during ice free months. The USGS Earth Explorer database search was limited to images with <40% cloud coverage that fell within the selected temporal range. For this study, Landsat-8 OLI data, Collection 1 Level-1 Landsat 8 OLI/TIRS was utilized. It must be noted that the USGS is reprocessing its collection management structure on January 1, 2022, so that all new multiband acquisitions will be processed into Collection 2. (Wulder et al. 2019) At the time of data processing for this project, the NASA program SeaDAS is unable process Landsat Collection 2 data however subsequent updates will hopefully make processing of collection 2 data viable. Collection 2 data has an improved usage of ground control points, greater cloud masking, and land characterization techniques specified for water confidence. (Landsat Mission 2021) Until the SeaDAS program can process collection 2, the methods outlined in this thesis are at a disadvantage until the tools used for ocean color processing are updated. SeaDAS also

requires either a Linux or MacOS operating system to conduct the Ocean Color Science SoftWare (OCSSW) processing. While NASA has released a version of SeaDAS that is compatible with a Windows system, it requires a virtual connection to a Linux server to run OCSSW and L2gen – requirements of the methods of this thesis. Another program that can be used to process R_{rs} is 'Atmospheric Correction for OLI 'lite', or ACOLITE, a generic processor developed by the Royal Belgian Institute of Natural Sciences to process reflectance and atmospheric correction within multispectral imagery. (RBINS 2021) There is a variety of computer programs and operating systems that could be used to complete a SDB map.

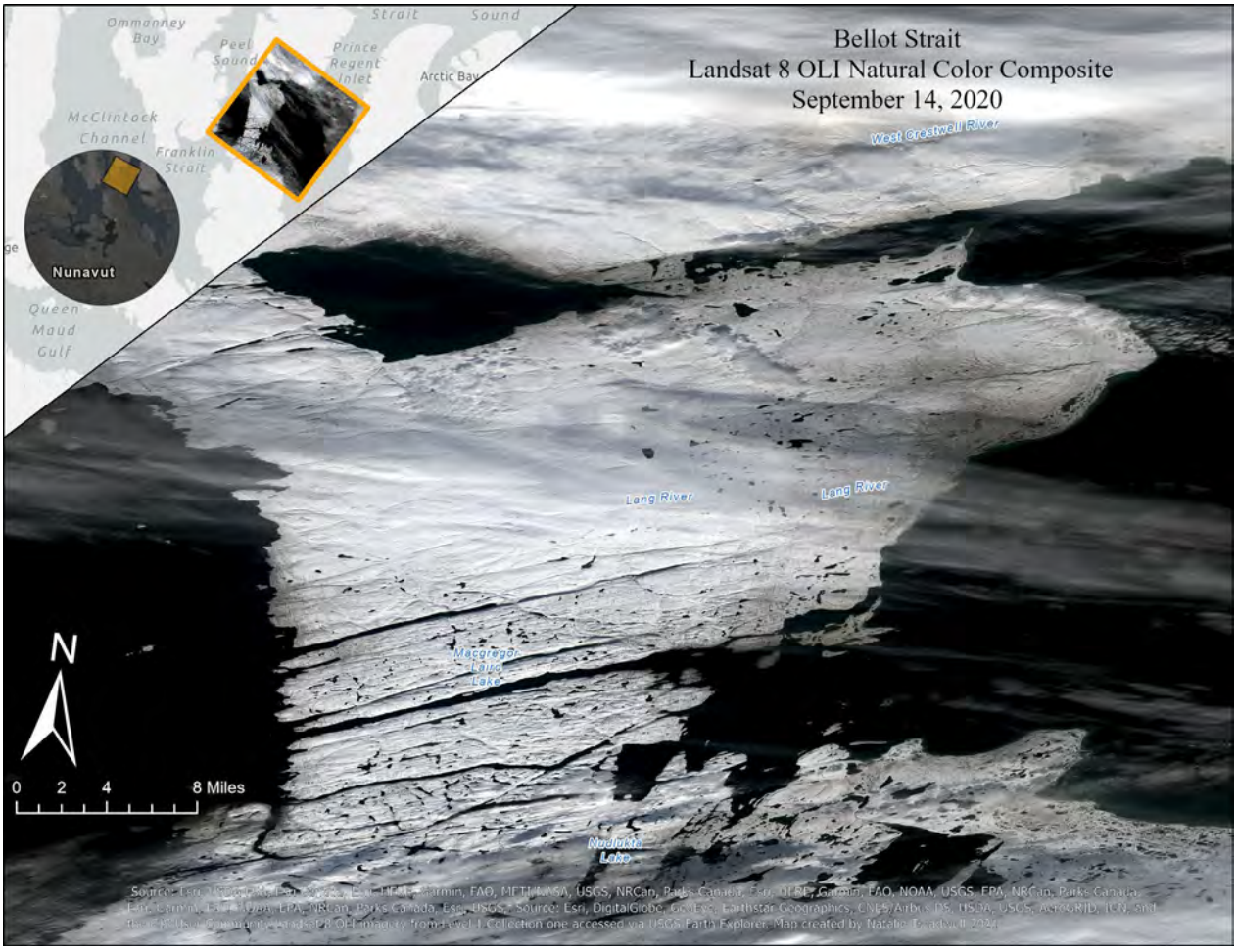

Figure 6: Landsat-8 OLI data covering the study area with >40% cloud coverage

While no multispectral imagery was produced on the 28th of August, imagery taken on the 29th of August containing >70% cloud coverage revealed that the area was ice free, meaning there is a high likelihood that OSW was free of ice at the time of ATL03 data collection. Level 1 Collection 1 Landsat 8 OLI/TRS data from September 14th was selected due to the large coverage of the Bellot Strait in one image as well as the clarity of pixels representing shoreline. The natural color composite shown in Figure 6 depicts the red (Band 4), green (Band 3), and blue (Band 2) and has been pansharpened using the 15m resolution panchromatic (Band 8). No preprocessing was done to the image before it was imported into SeaDAS, which can only process level one collection one from Landsat-8 OLI, therefore the Level-1 GeoTIFF Data Product was accessed via EarthExplorer by the USGS (EarthExplorer 2020). Data access can be acquired through any web browser and downloaded as TIF files or HDF5 for Landsat-8 and ICESat-2 respectively. Email registration is required for both USGS EarthExplorer and OpenAltimetry to download data; the whole collection of raw data should be chosen for this process. MATLAB can be accessed via their developer, Mathworks, along with the needed 'add-ons' such as the computer vision toolbox, image processing toolbox, statistics and machine learning toolbox, signal processing toolbox, and the curve fitting toolbox.

3.2. Pre-Process Data

In many cases, tidal harmonic analysis, or using algorithms developed to model amplitude and phase of tides, is necessary to match the tidal cycle of the multispectral and LiDAR data. (Lee et al. 2021) In a serendipitous case, both datasets were taken during a period where the tidal station located at the East entrance of the Bellot Strait recorded tides as +0.6 m at 1:02pm on August 28th, 2020 for the ICESat-2 data and as +0.58 m at 6:11pm on September 14th,

2020 for the Landsat 8 OLI data. (Government of Canada DFO, 2021; NSIDC, 2021; NASA EARTHDATA 2021) Considering the difference in tides was a negligible 0.02 m, the decision was made to omit harmonic tidal analysis from the methods of this thesis. Lee et al. (2021) suggests the use of the MATLAB model T_Tide, developed by University of British Colombia's Ocean Dynamic Laboratory researcher Rich Pawlowicz, when tidal analysis is required in other SDB models. (Pawlowicz, 2011) After the datasets have been evaluated for tidal cycle harmony, pre-processing of the multispectral reflectance can continue.

The NASA Sea Data Analysis Software (SeaDAS), created to process ocean color data, is leveraged here to process reflectance from the Level 1 Landsat-8 OLI data. The program is specifically built to apply atmospheric correction and calculate reflectance of multispectral images of water. The pre-processing of the Landsat data also removes features such as land, clouds, ice, and sun glit while providing the reflectance of raster cells which meet suitability requirements set by SeaDAS. The Level-2 processing (L2gen) can apply hundreds of different product options for output, including remote sensing reflectance (R_{rs}), which estimates the near-infrared water leaving reflectance from Landsat-8 OLI data. Under processing options, aerosol calculation 'aer_opt = -2' is used the employ equation (1) developed by Bailey et al. (2010)

$$R_{rs\,(}\lambda) = G_{(}\lambda) \times X\,(\lambda) \qquad (1)$$

Table 1: Reflectance correction variables

$R_{rs}\,(\lambda)$	Reflectance
$G(\lambda)$	Function of the illumination conditions, sea-state, and water constituents.
$X(\lambda)$	$X(\lambda) = \frac{b_{b(\lambda)}}{a(\lambda)+b_b(\lambda)}$

$b_b(\lambda)$	Backscattering coefficient: $[b_{bw(}\lambda) + b_{bp}(\lambda)]$
$a(\lambda)$	Absorption coefficient: $[a_w(\lambda) + a_p(\lambda) + a_g(\lambda)]$ Where the subscripts w, p, and g represent contributions by water, particles, and dissolved material.

The L2gen R_{rs} outputs are also processed to mask land features, cloud or sea ice contamination, high or saturated radiance, and strong sun glint contamination. The output is four distinct raster layers representing ocean surface R_{rs} in the coastal aerosol, red, green, and blue bands.

3.2.2 ICESat-2 ATL03

The ICESat-2 ATL03 data comes in a hierarchical data format version 5 (HDF5 or.h5) file where the ellipsoid heights (H) are segmented from the ground tracks. To limit unreliable photon returns, only photon returns from the strong ground tracks will be used. The dataset also suggests the substrate which the photon interacted with using an onboard sensor and ground-finding algorithm to assign confidence values within five landcover types. The five columns represent surface types which the photon events are associated with, the landcover types are land, ocean, sea ice, land ice, and inland water (1-5 respectively). Signal confidences are represented by a 5xN matrix where N is equal to the number of photons returns: -2 for returns within the transmitter echo path (areas where laser strength is weak), -1 for events that could not be associated with a surface type, 0 for signal noise, 1 for background noise, 2 for low confidence, 3

for medium, and 4 for high. (Neumann, 2019) Data points with signal confidence lower than 3 in the classification column ‘ocean’ (column 2) are ignored to ensure that background noise would not be included in the training data.

The Icesat-2 data product must then be projected from its reference frame WGS84/ITRF2014 (Neumann et al. 2019) to the Canadian Geodetic Vertical Datum (CGVD2013) to reproject the heights as orthometric rather than ellipsoid heights as provided in the raw .h5 file. The raw ATL03 points will depict a noticeable tilt if they are not corrected to orthometric heights in accordance with the geoid gravity model developed by Natural Resources Canada (NRCan 2020). When projecting ocean surface in ellipsoid heights there is a noticeable tilt that can be observed when isolating point cloud data over the ocean. The main factor is the ellipsoid heights are referenced to a flattened sphere (ellipses) used to represent a geometric sphere of the world, referenced to mean sea level. Since the geoid of the earth is irregular, in some areas of the world and especially in the poles, heights referenced the ellipsoid can distort bathymetric heights as much as several meters off the geoid. ICESat-2 data provides a photon height reading of *H* as referenced to ellipsoid heights, therefore it must be converted to orthometric values. (Esri 2003) The tool, GPS-H created by NRCan is used to covert ellipsoid heights to orthometric values. The study conducted by Babbel and Parrish both project the photon points to the earth gravitational model EGM2008 using VDatum, a tool developed by NASA to convert ellipsoidal heights to orthometric. (Parrish et al. 2019; Babbel et al. 2021). While other studies utilized a global gravity model, VDatum was initially leveraged and was found to overcorrect the photon returns and removed most of the bathymetric points. Careful considerations should be made regarding the type of projection to ensure the datum conversion is

in accordance with the unique study area and offers the most geographically correct orthometric height values.

Once the photon returns have been converted to Canadian reference system, equations 1-11 from Parrish et. al (2019) were adapted to perform the refraction correction. The order of the equations has been rewritten for clarity in this study and ease of calculation within the MATLAB code respectively and are rewritten here as equations 2-14. Some variables were defined by Parrish et al. (2019) in a list and they have been adapted in this thesis to demonstrate the equation rather than describing how to calculate said variables.

$$\theta_1 = \frac{\pi}{2} - ref\_elev \tag{2}$$

Ref_elev can be found in the HDF5 files and the mean value is used as a constant.

$$\theta_2 = \sin^{-1}\left(\frac{n_1 \sin\theta_1}{n_2}\right) \tag{3}$$

n_1 and n_2 are estimates of the refractive indices of air (n_1) and water (n_2). The default refractive indices of air was adopted from Parrish et al. (2019) where (n_1 = 1.00029) and the indices of water was calculated to be (n_2 = 1.343).

$$S = \frac{h}{\cos\theta_1} \tag{4}$$

Where h is derived from the height of seafloor returns segmented from the ATL03 dataset. Equation five accounts for the change that occurs to the speed of light when passing though the

interface of air and water. Considering the LiDAR laser moves differently through water than it does air, equation five corrects the change in laser speed which was not initially accounted for in the raw ATL03 data.

$$R = \frac{Sn_1}{n_2} \tag{5}$$

Equation five uses the same refractive indices of water used in equation three. The following geometric refraction correction rely on the law of sines, cosines, and other trigonometric functions to compute the change in longitude (ΔY) and height (ΔZ). Figure 7 is taken directly from Parrish et al. (2019) and visually explains the horizontal and vertical corrections applied through the refraction correction.

Variables:

$$\gamma = \frac{\pi}{2} - \theta_1 \tag{6}$$

$$\emptyset = \theta_1 - \theta_2 \tag{7}$$

Law of cosines:

$$P = \sqrt{R^2 + S^2 - 2RS\cos\emptyset} \tag{8}$$

Law of sins:

$$\propto = \sin^{-1}\left(\frac{R\sin\emptyset}{P}\right) \tag{9}$$

Solve for the angle made from ΔY, ΔZ, and P

$$\beta = \gamma - \alpha \quad (10)$$

Calculate the remaining offsets:

$$\Delta Y = P \cos \beta \quad (11)$$

$$\Delta Z = P \sin \beta \quad (12)$$

The final step is to apply the same offset of ΔY on all latitude and longitude coordinates (represented as ΔE for latitude and ΔN for longitude). The final variable *k* is calculated using the mean value from ref_azimuth and represents the reference azimuth of the photons vector.

Horizontal Offset:

$$\Delta E = \Delta Y \sin k \quad (13)$$

Vertical Offset:

$$\Delta N = \Delta Y \cos k \quad (14)$$

The result of these equations is a dataset of photon H returns that have been corrected for refraction and the respective change in latitude and longitude that occurs in accordance with the refraction correction. Any photon returns that are positive values are then omitted from the study to isolate bathymetric points; 1,225,444 photon returns were processed through refraction

correction and 390,140 of those points contained bathymetry ranging from 0-34 m below sea level.

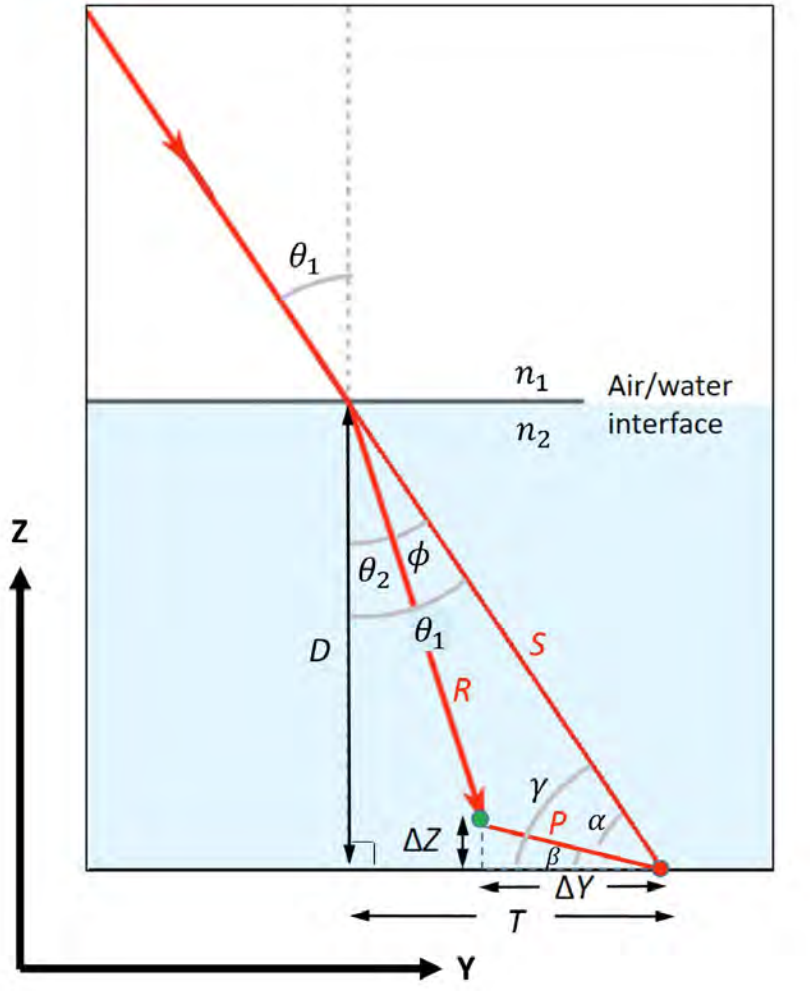

Figure 7: Model displaying the geometry of the refraction correction Parrish et al. (2019)

The two preprocessed datasets, bathymetric photon returns, and reflectance multispectral layers are then collocated using by associating ICESat-2 height measurements (referred to as H_{LiDAR}) to the Landsat-8 OLI raster based on the closest distance. All ICESat-2 data points within a OLI pixel will be used to calculate the mean H values and generate the optically shallow

depth index. H_{LiDAR} will serve as the tuning parameters that influence the satellite-derived bathymetry equation.

3.3. SDB

The main spatial analysis is applying the multiband value algorithm (MBVA) and the two-band ratio algorithm (TBRA), which both leverage reflectance and LiDAR training points to interpolate depth across the surface. These equations are validated by calculating the error and evaluating how these errors could be exaggerated by the conditions unique to the study area. Other studies have used multibeam sonar readings to validate the findings however that data is unavailable for the Bellot Strait. While complete precision is not possible with this method, general accuracy is expected when using ICESat-2 data to train the model.

3.3.1 Multiband Value Algorithm (MBVA)

The following equation will be applied to the Landsat-8 data in MATLAB to solve for H_{imger} which is the satellite derived bathymetric representation.

MBVA:

$$H_{imager} = \alpha_0 + \sum_1^N \alpha_i \ln(R_{rs}(\lambda_i)) \quad (15)$$

Table 2: Multiband Value Algorithm variables

$\alpha_{0\text{-}i}$	Empirical coefficients derived from collocated R_{rs} and ICESat-2 data
$R_{rs}(\lambda_i)$	$R_{rs}(\lambda_i)$ is the reflectance of wavelength calculated from the Landsat-8

This equation is used to prove that the log of the difference of reflectance is proportional to the depth of the water.

3.3.2 Two band Ratio Algorithm

The two-band ratio algorithm, equation sixteen, developed by Stumpf et al. (2003) and fitted to use ICESat-2 LiDAR data by Lee et al. (2021) is used to calculate the ratio of the blue and green bands to estimate height. This method is good for areas with dark bottom substrates where the difference between reflectance and optically deep water could be negative.

TBVA:

$$H_{imager} = a_o + a_i\left(\frac{\ln(3.14nR_{rs}(\lambda_i)}{\ln(3.14nR_{rs}(\lambda_j)}\right) \quad (16)$$

Table 3: Two Band Ratio Algorithm variables

$\alpha_{0\text{-}i}$	Empirical coefficients derived from collocated R_{rs} and ICESat-2 data
$R_{rs}(\lambda_i)$	$R_{rs}(\lambda_i)$ is the reflectance of blue wavelength calculated from the Landsat-8
$R_{rs}(\lambda_j)$	$R_{rs}(\lambda_j)$ is the reflectance of green wavelength calculated from the Landsat-8
n	Fixed constant of 1000.0 recommended by Lee et al. (2021). This value can range from 500-1500 depending on the type of substrate

Finally, mean square error (MSE), tStat and P value are calculated and evaluated for both the MBVA and the TBVA to understand the statistical significance of the spatial model. The MATLAB code used to complete the equations outlined in Chapter 3 is included in Appendix B.

Chapter 4 Results

4.1. SeaDAS outputs

The results of the SeaDAS L2gen processing are shown in Figure 8 depicting the R_{rs} from four bands, coastal aerosol (443 nm), blue (482 nm), green (561 nm) and red (655 nm). The colored pixels represent areas of ocean that contain reflectance in accordance with the atmospheric correction and reflectance calculations included within L2Gen processing. Areas of land, sea ice, cloud coverage, and poor reflectance has been omitted and are represented by white pixels.

Visual interpretation of the SeaDAS output reveals that the red band contains more noise than other three bands and contains negative reflectance values. Using the reflectance correction model derived by Bailey within the L2Gen processing can lead to negative R_{rs} values in the near-infrared and short-wave infrared bands, which can be interpreted as low sensitivity of sensors, and high absorption of red, SWIR, and NIR light in water.

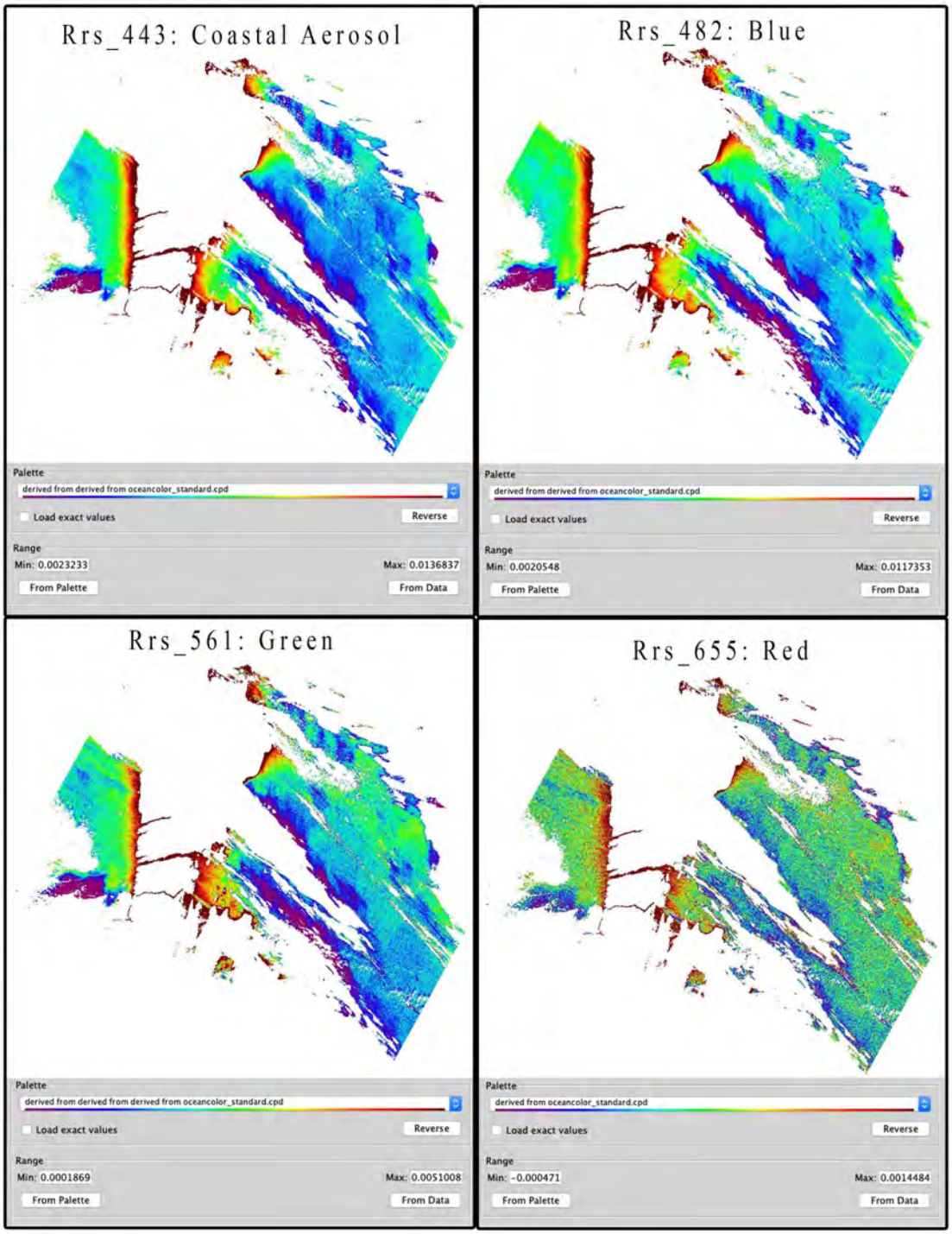

Figure 8: R_{rs} values calculated through SeaDAS

4.2. ATL03 Refraction correction

Figure 9 shows the Landsat 8 OLI imagery with the ICESat-2 ATL03 photon returns overlayed. The three strong ground tracks are displayed over the Landsat 8 image to show where the LiDAR depths were recorded.

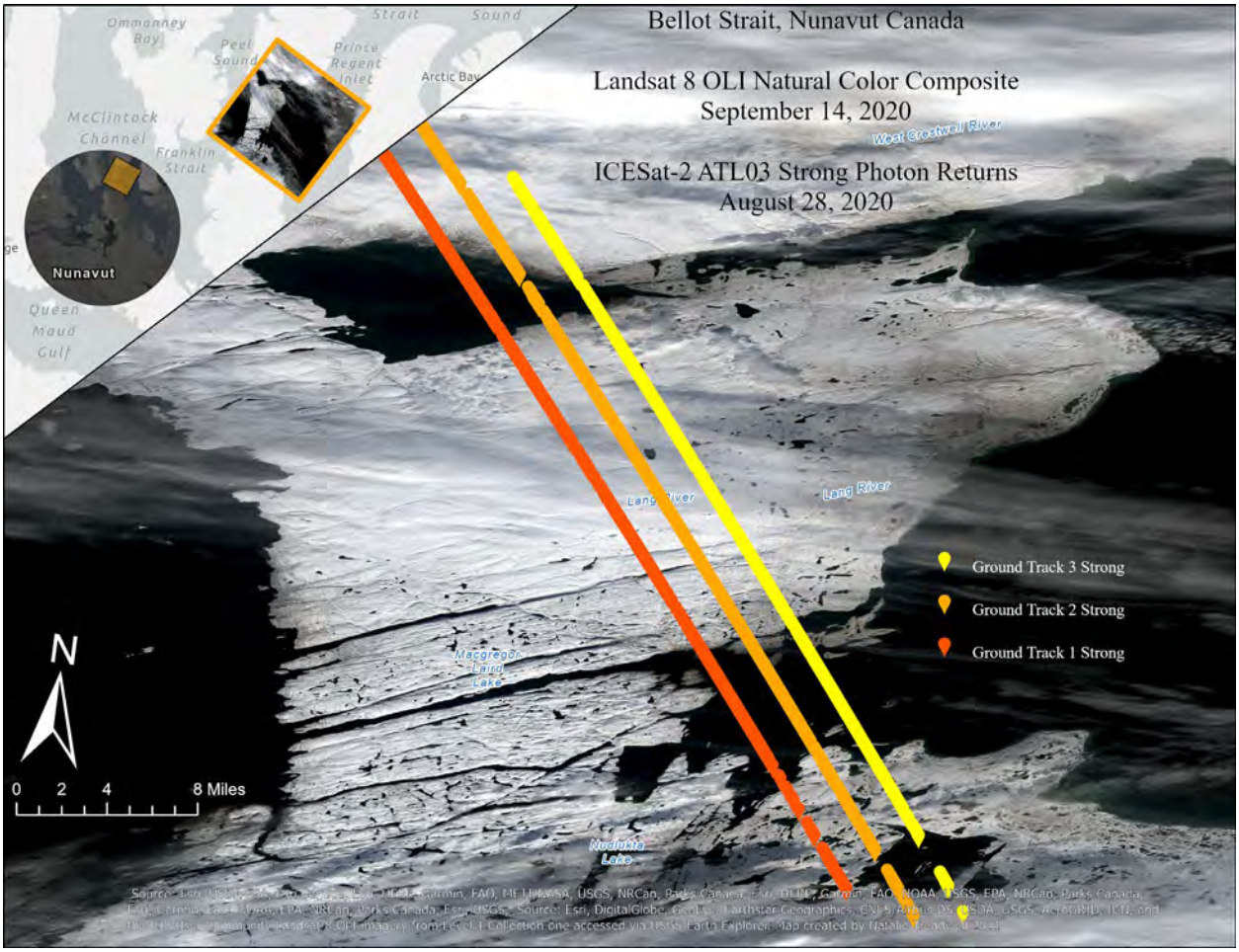

Figure 9: Landsat 8 OLI and ICESat-2 ATL03 Ground Tracks 1-3 Strong

After converting the ATL03 tracks to orthometric height values, any photon points above 0 m sea level and below 23 m were removed to isolate the remaining bathymetry. Photons below

-23 m are considered noise due to their high concentration of returns and general lack of reliability in LiDAR depths after -20 m.

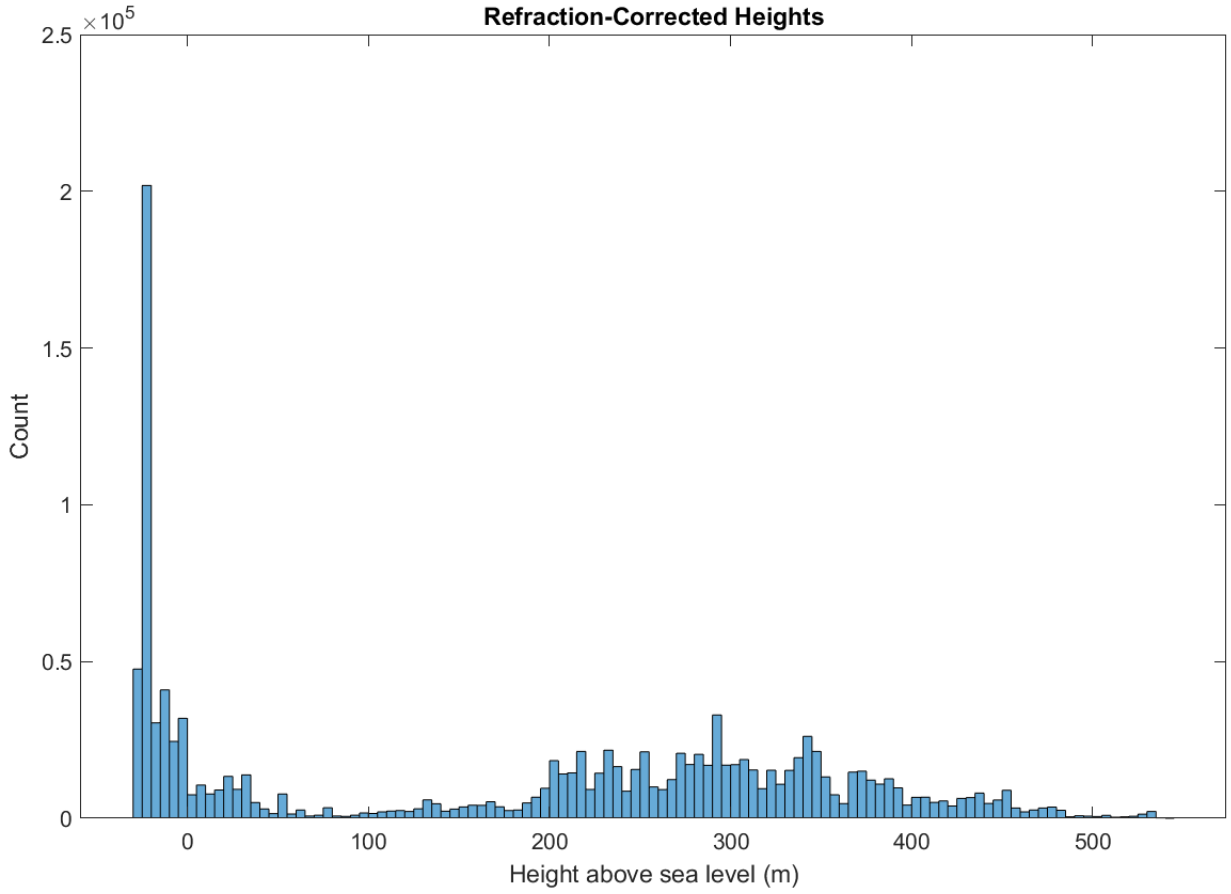

Figure 10: All ATL03 Refraction Corrected Photon Returns

Shown in Figure 10 is the distribution of points after refraction correction and before the bottom outliers were removed. The data represented in Figure 10 contains all heights above sea level, which show the highest elevation recorded in the dataset to be greater than 500 m. Figure 11 shows the total distribution of height values among all ATL03 strong ground tracks with a signal confidence of 3 or higher. It also shows the data after outliers have been removed to represent heights recorded below sea level and the distribution of training bathymetry. Many outliers began around -24 m therefore the data is clipped to only include values between 0-23 m of depth. The model is highly dependent on the training data and a statistically significant model was not

achieved until the outliers were removed. The final training collocated ATL03 photon return uses are shown in Figure 11.

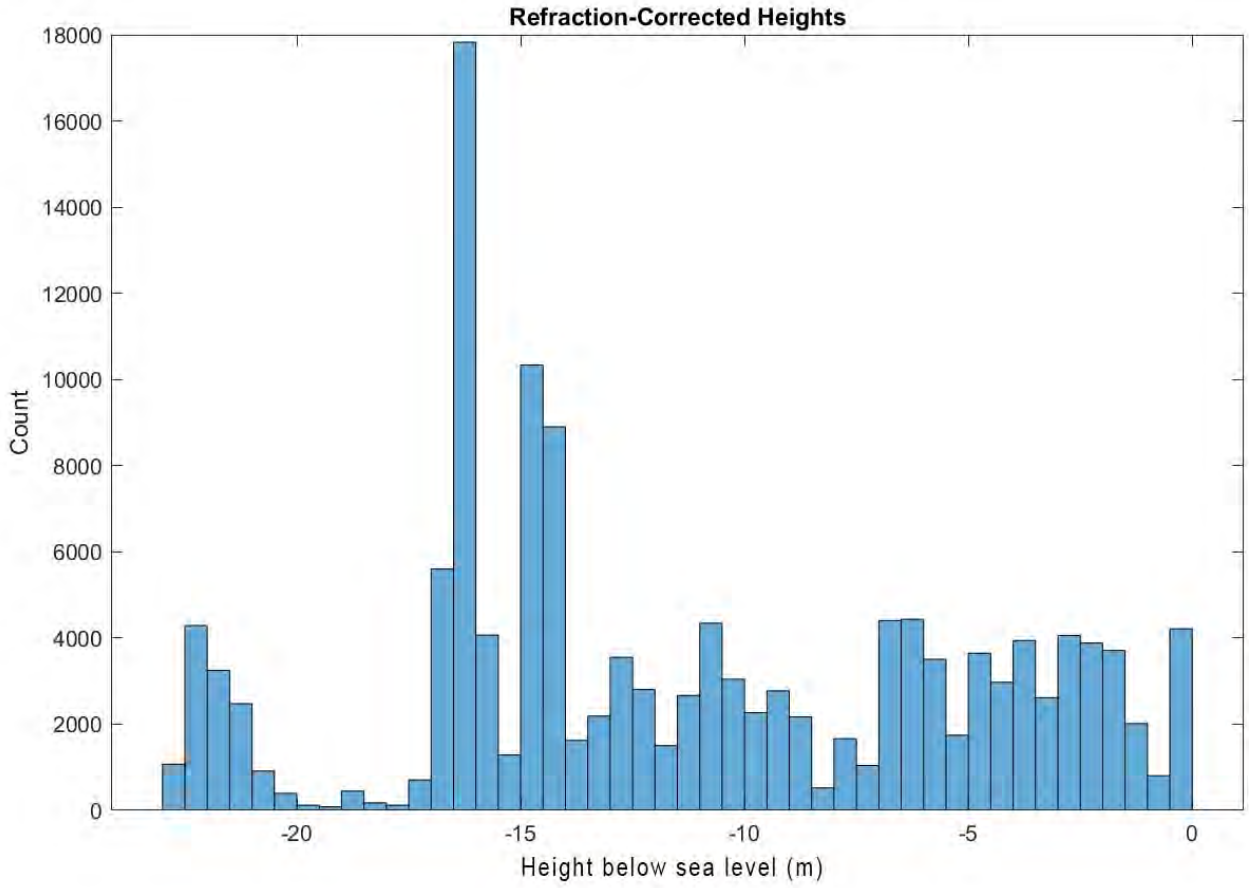

Figure 11: ATL03 Bathymetric Photon Returns used in Collocation Training.

4.3. Multiband Value Algorithm

The multiband value algorithm used the coastal aerosol, blue, and green bands to calculate depth. The algorithm was fit to a linear regression and close ups of the Bellot Strait and Creswell Bay to the Northeast of the strait are shown in Figures 12-13.

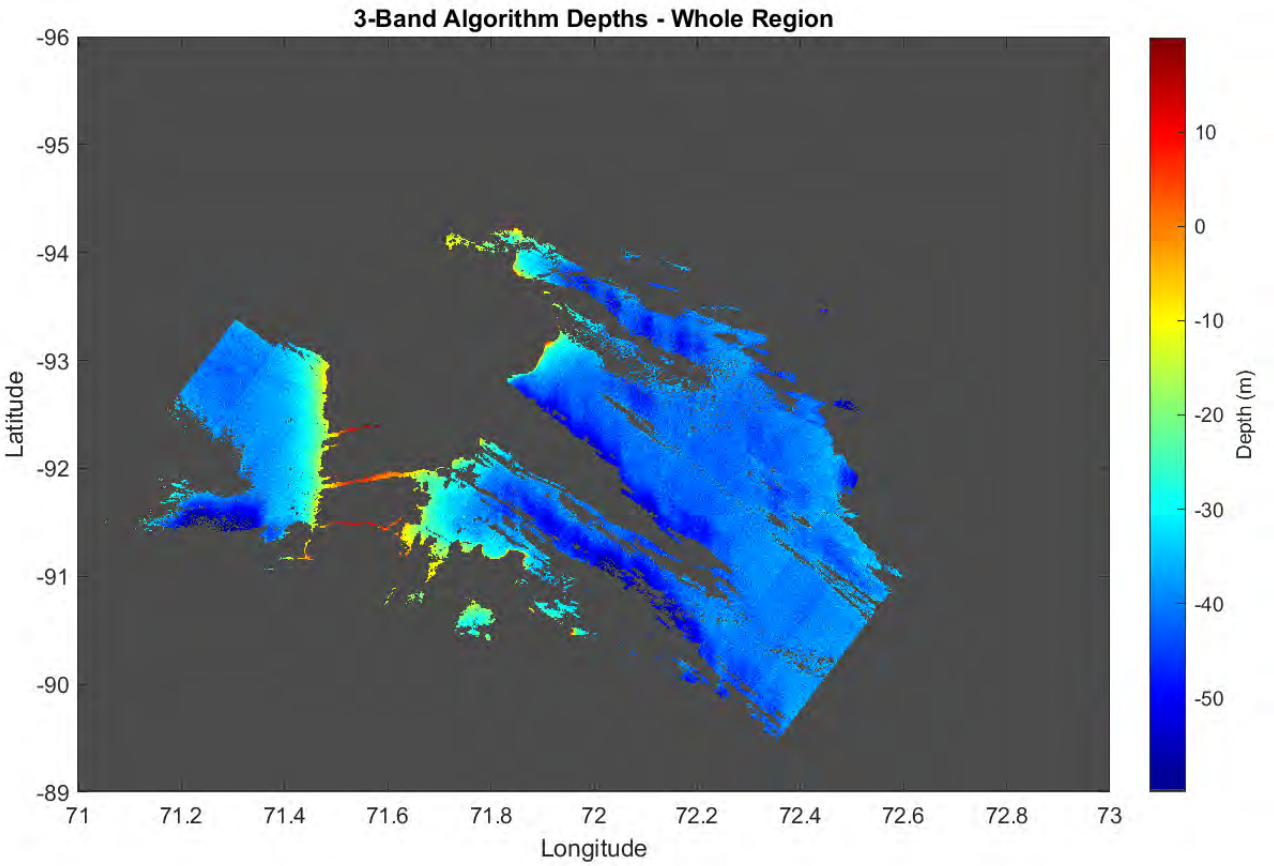

Figure 12: Results of the MBVA

Table 4: Statistical Measures of Confidence for MBVA

RMSE	1.16 m
r^2	0.945 m
Adjusted r^2	0.913 m
P value	0.00139

Table 5: Estimated Coefficients of Linear MBVA

α_0	534.71
α_1	225.01
α_2	-101.11
α_3	-12.467

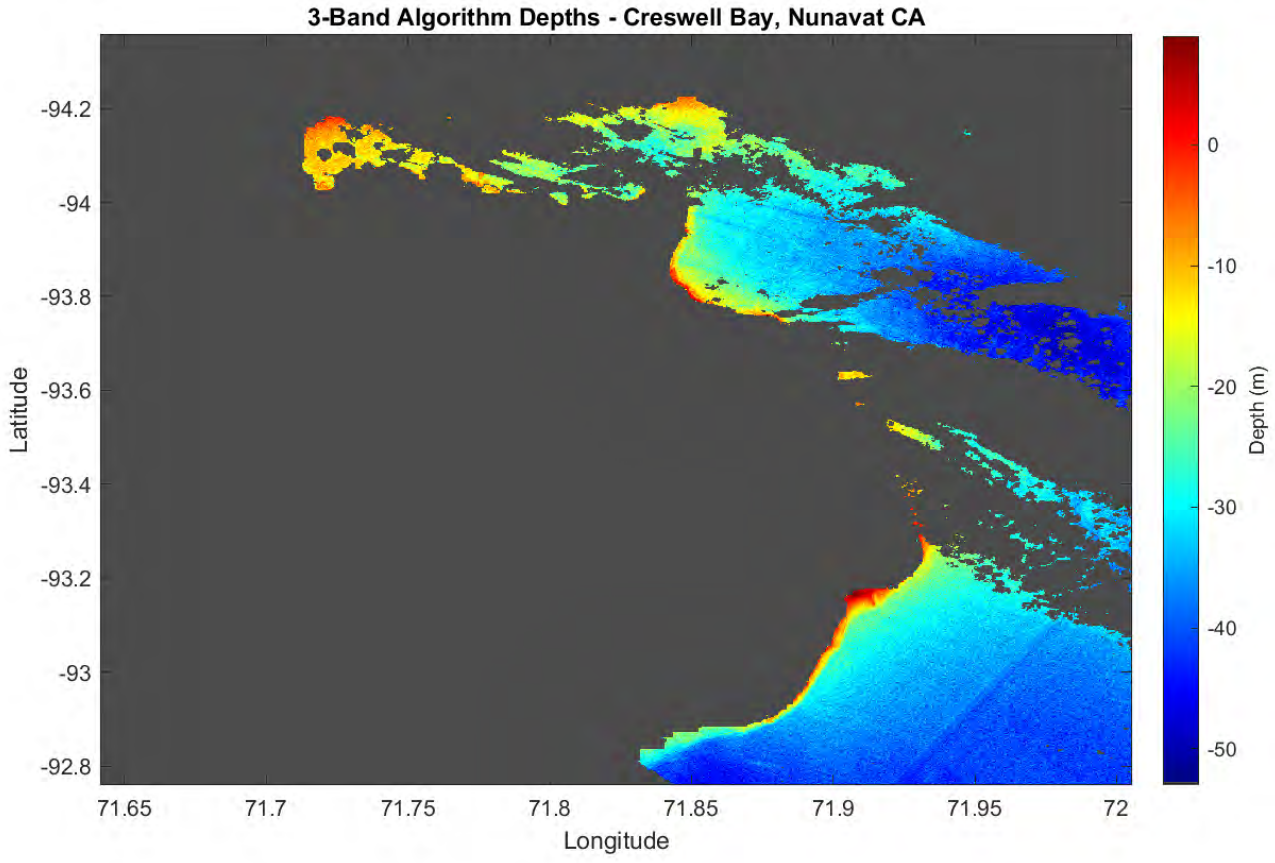

Figure 13: MBVA depths in Creswell Bay, NE of the Bellot Strait

Creswell Bay is another area in the study area that returned clear bathymetric returns between depths of 10-20 m. Creswell Bay, like the Bellot Strait, is not comprehensively mapped, therefore this bathymetric model shows that in general, the bay is navigable but great caution should be taken in the inlet which it leads into. Some interpretation is needed to see the difference between coastline and cloud cover.

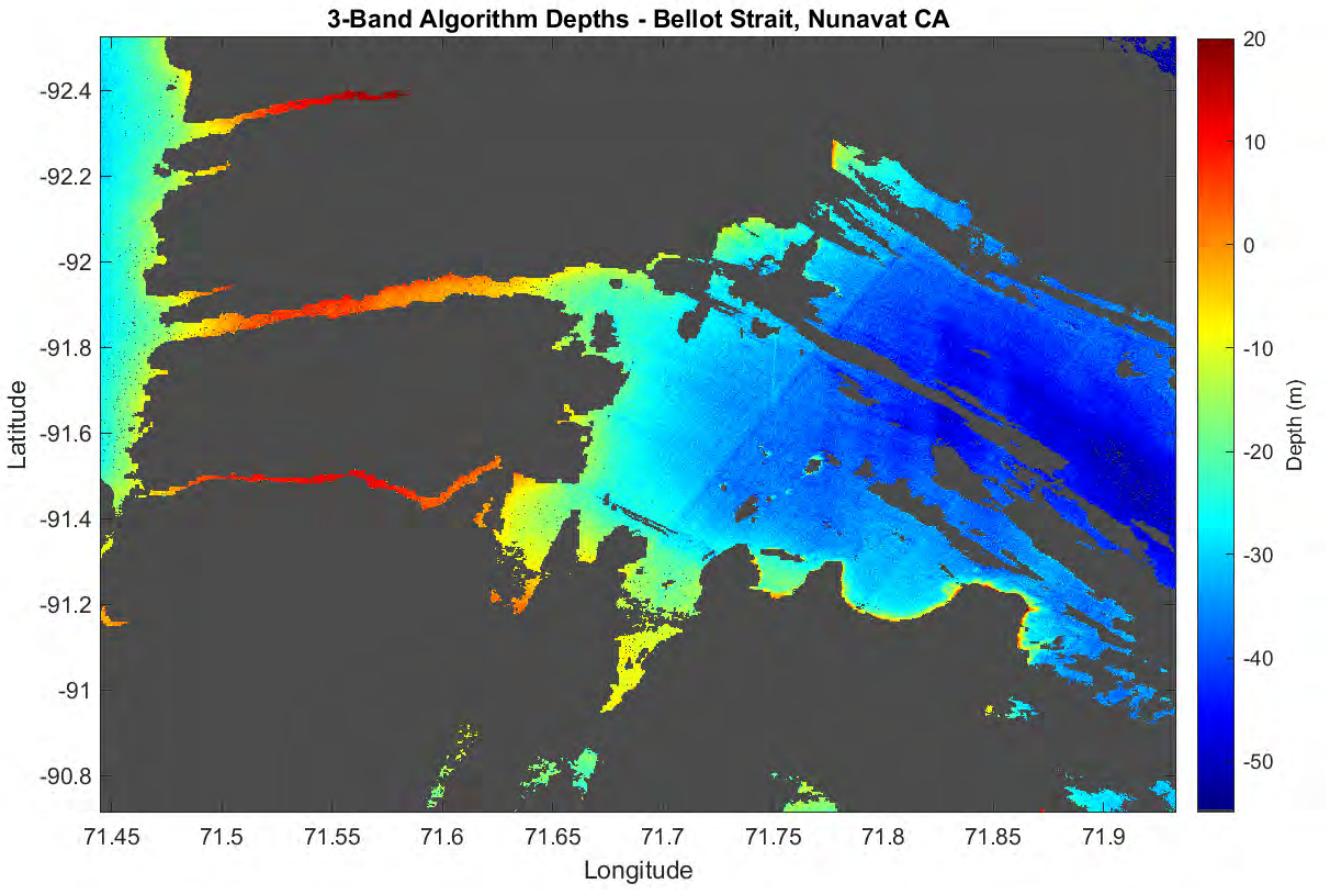

Figure 14: SDB using MBVA in the Bellot Strait

The depths interpolated through the MBVA show a range between 10 m and -50 m of depth, the depths outside of the training data (0-23 m) was extrapolated by the model and shows a distribution of predicted deep water points, shown in Figure 15. Unfortunately, any depths past 20 m cannot be verified with training data and it is known from the NONNA data that depths up

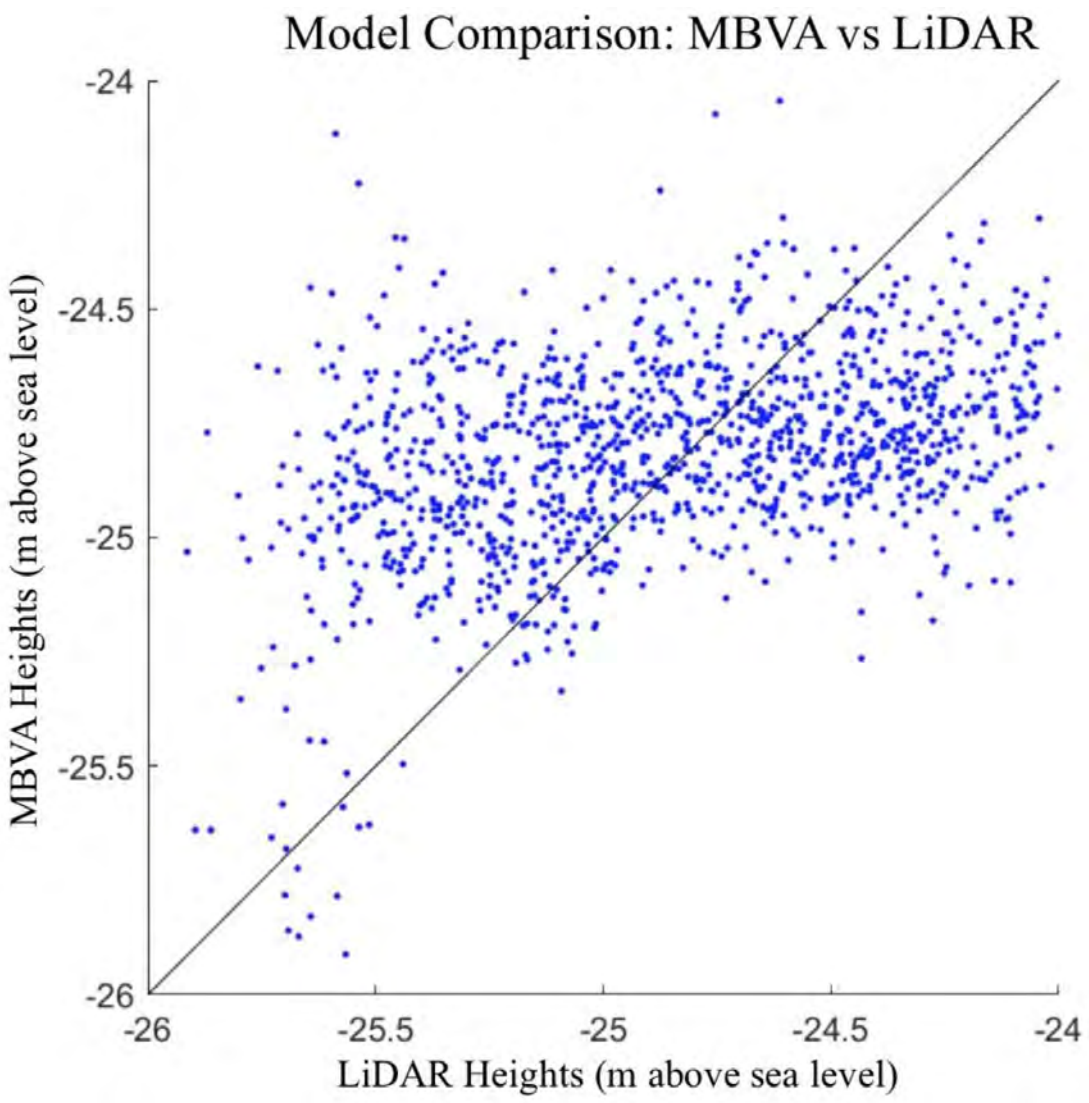

Figure 15: Model Comparison: Multi-band vs LiDAR

4.4. Two Band Ratio Algorithm

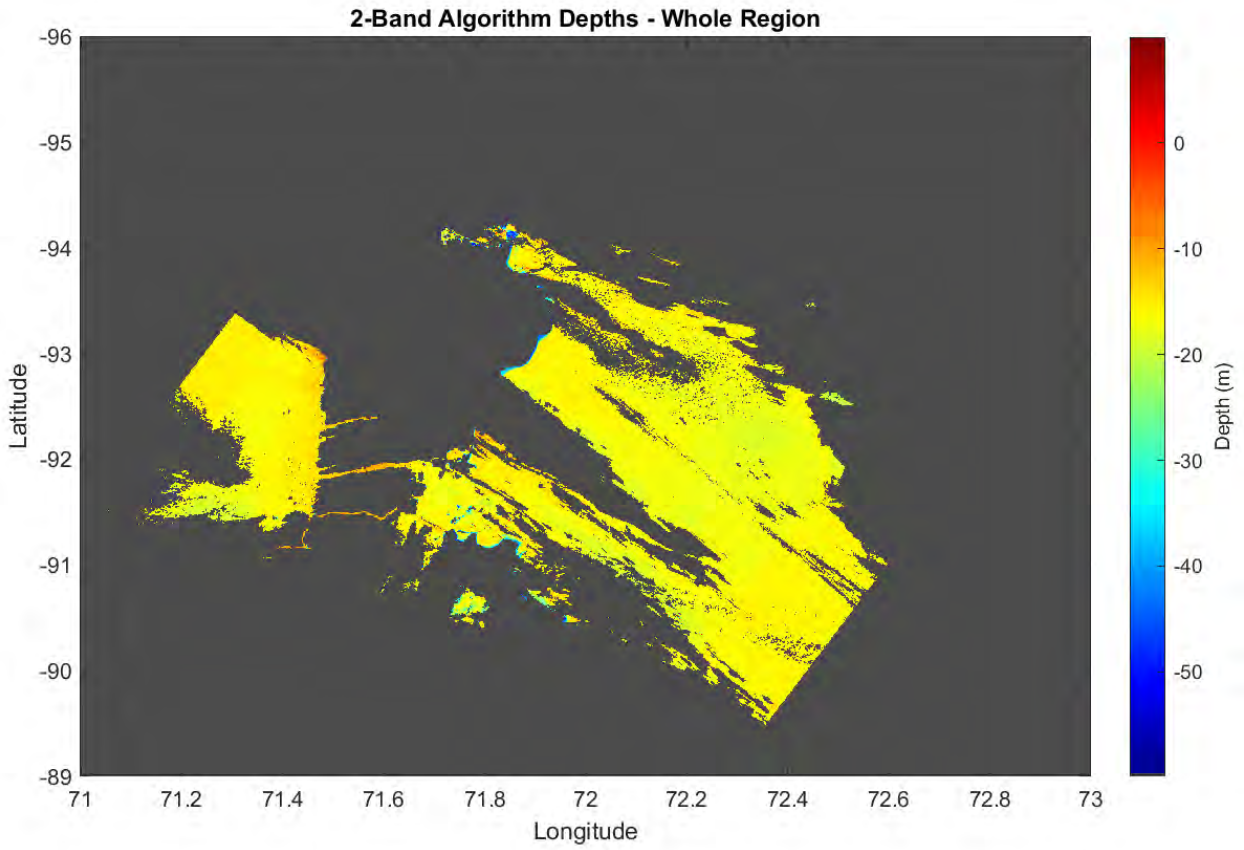

Figure 16: Results of the TBVA

The Two Band Ratio Algorithm used the blue and green wavelengths to calculate bathymetry. The greatest difference between the TBVA and the MBVA is how the model assigned depth in unknown deep waters. In the MBVA, deeper water was assigned to a value of < -30 m whereas deep water in the TBVA was assigned a depth of around -20 m. Because the MBVA model extrapolated depths that were not present in the training Icesat-2 LiDAR data, the TBVA could have modeled the deep-water threshold better. It is difficult to determine which model did a better job at predicting deep water, however the MBVA has a clearer distinction

between water that is classified as 20 m and deeper water, whereas the TBVA does not clearly define the shift to deeper water.

Table 6: Statistical Measures of Confidence TBVA

RMSE	2.38 m
r^2	0.675 m
Adjusted r^2	0.629 m
P value	0.00659

Table 7: Estimated Coefficients of Linear TBVA

α_0	500.15
α_1	-660.52

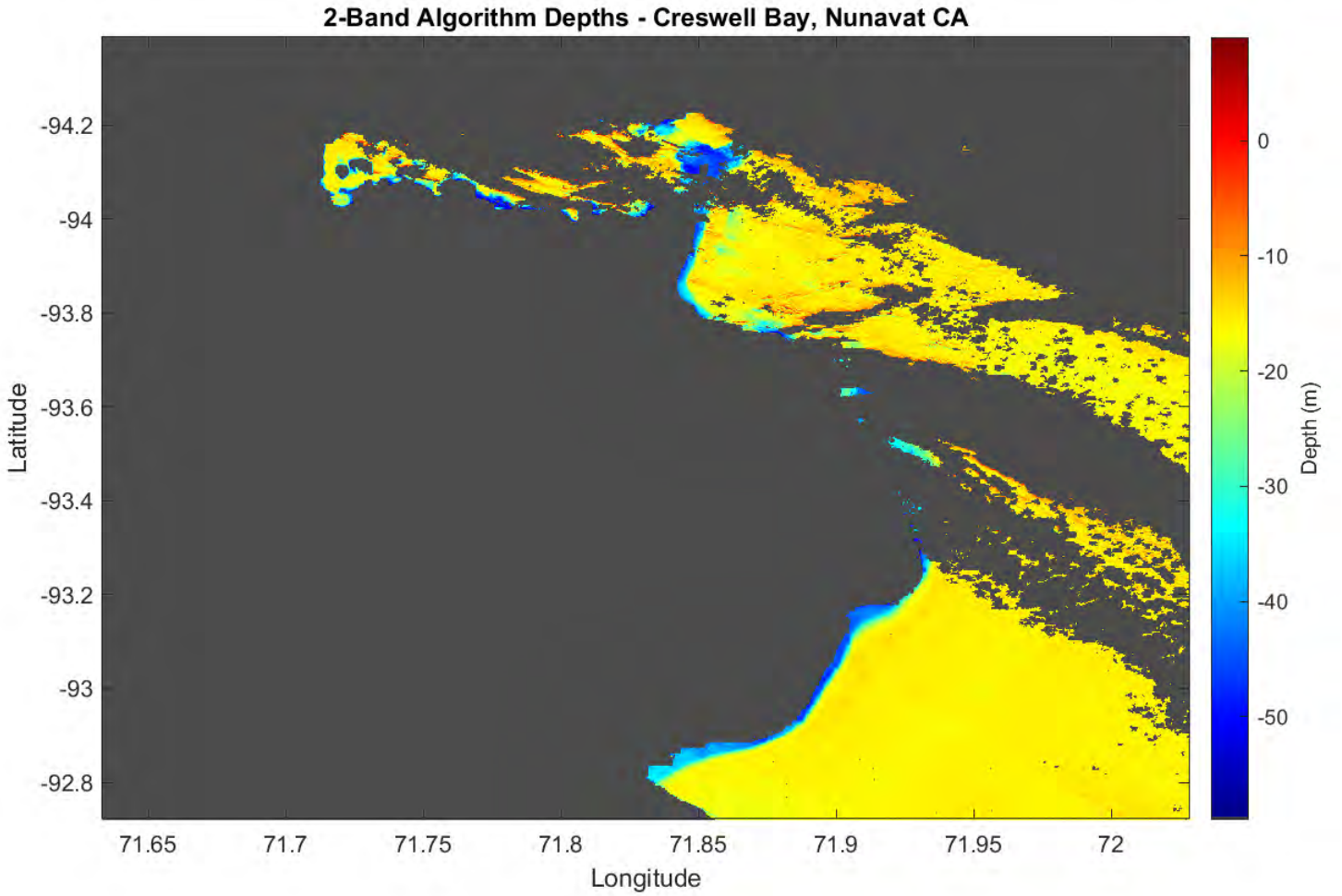

Figure 17: TBVA of Creswell Bay, NE of the Bellot Strait

Upon closer inspection, it seems that the TBVA did not capture bathymetry well in Creswell bay compared to the MBVA, which saw a greater density of depths between 10-20 m of depth along coastlines. Similar trends were noticed when comparing MBVA and TBVA in the

Bellot Strait, greater certainty is found near shoreline in the MBVA as opposed to depths of -30 m being recorded near the shoreline in the TBVA.

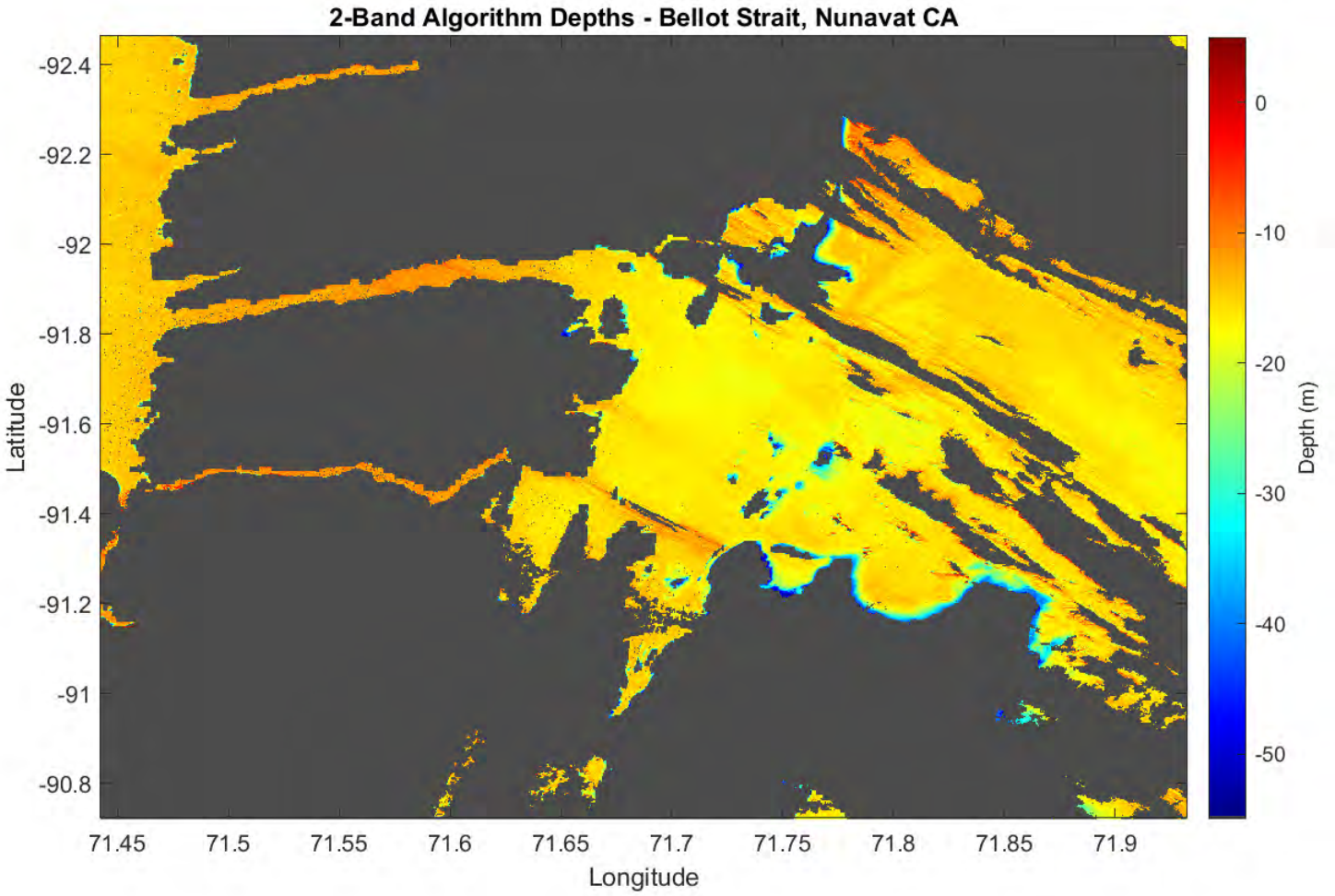

Figure 18: TBVA in the Bellot Strait

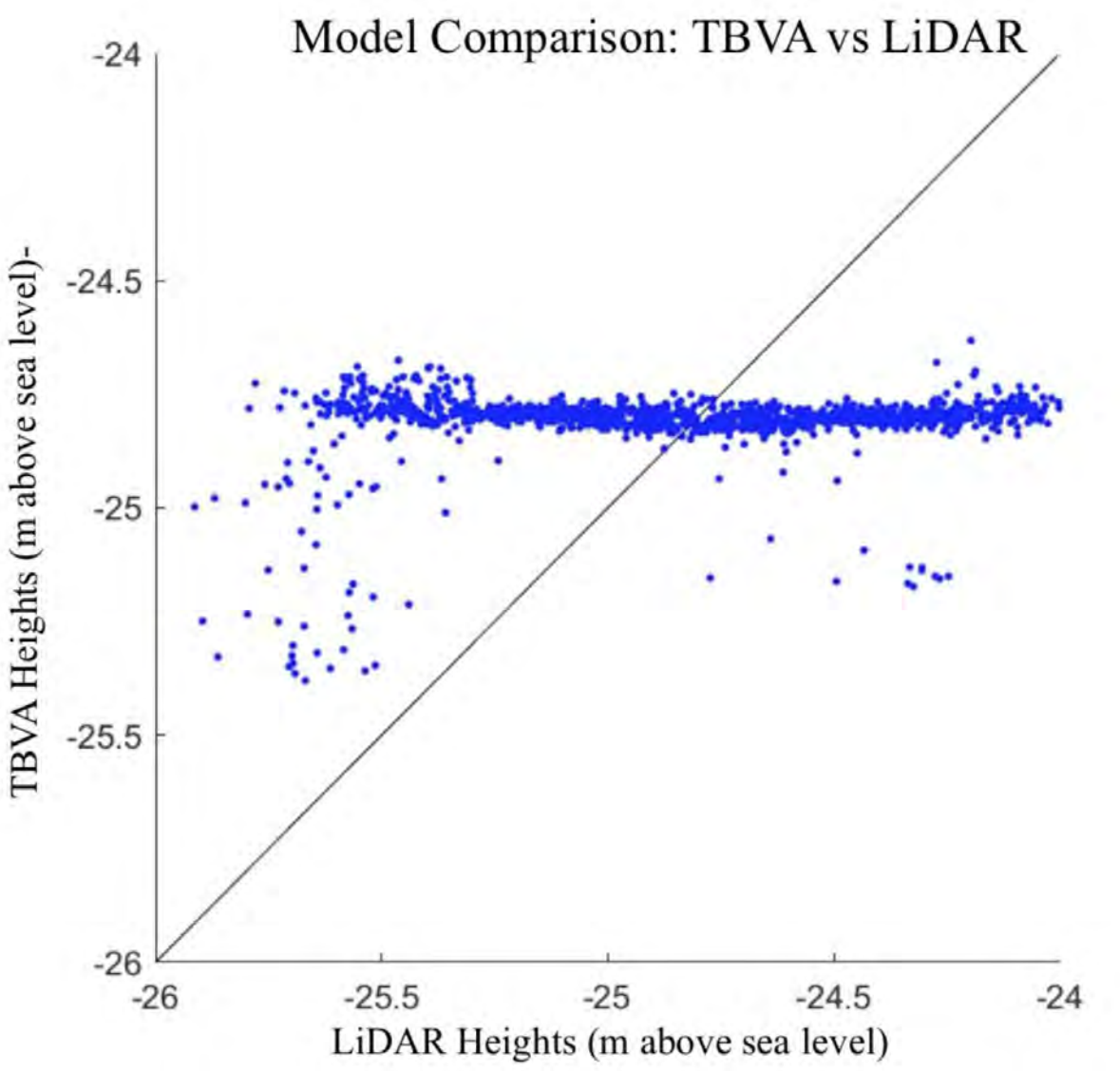

Figure 19: Model Comparison: Two-Band vs LiDAR

Figure 19 shows the distribution of the LiDAR heights acquired from the ICESat-2 satellite after refraction correction versus the heights predicted by the TBVA. As it can be seen in the map interpolations, most of the data is concentrated between -24 m and -25 m of depth. This figure can help explain the extrapolation that occurred in the TBVA model that classified deep water as between -20 m and -30 m of depth.

Chapter 5 Discussion

The developmental goal of this thesis is to measure the applicability of the SDB model in the Bellot Strait using ICESat-2 LiDAR derived depths. Despite the many technological and geospatial challenges that come with creating a SDB chart, the goal was to apply the necessary corrections to space-based LiDAR to generate bathymetric training data for the multi-band value algorithm and the two-band value algorithm within Arctic conditions. The Bellot Strait was chosen to test this case due to its relevance to maritime activities and a large density of coastline within a small area. The intentions behind this choice were to test the MBVA and TBVA on a section of remote coastline that still has relevance to both Canadian and International maritime activities and that which contains a varying type of coastline within the spatial bounds of a single Landsat 8 OLI image. The Bellot Strait fit these conditions due to its wide variety of coastal inlets, exposure to two different bay systems, and significant marine traffic from August through September when the area is ice free. Another consideration for this area was the lack of Bathymetric data available within the surrounding areas of the Bellot Strait despite its widespread use as a corridor between the Gulf of Boothia and the Peel Sound. The primary challenge to accomplishing this spatial analysis is access to clear data – cloudless and ice-free days are far and few between in the Arctic. Other challenges stem from the solar zenith angle, access to software and hardware, and reliability of the SDB model, all variables that can drastically affect the error analysis of the SDB algorithms. After greater understanding of the SDB process, other ICESat-2 ground tracks across the Canadian Archipelago were surveyed to determine the potential coverage of this method.

5.1. Data Reliability

The ICESat-2 satellite has a 91-day repeat cycle for any given ground track location each location is surveyed an average of four times a year. With three years in orbit, the ICESat-2 satellite has only had the chance to pass over a unique location on a ground track an average of twelve times. There are five ground tracks that cross over coastline in the Bellot Strait – equating to a total of fifty-seven datasets over the study area, nine of which contained surveys conducted in August or September. Of those nine, only one dataset in the Bellot Strait contained bathymetric photon returns. (Khalsa et al. 2020). The ICESat-2 dataset that contained bathymetric photon returns was recorded on August 28th, 2020, limiting the search of Landsat 8 OLI data to imagery taken within a 32-day buffer. Considering the Landsat 8 OLI has a repeat cycle of 16 days, the buffer was established to increase the likelihood of quality imagery and ensure imagery was mostly ice free. Data filters were set within the USGS Earth Explorer program to restrict results to imagery taken between July 28th and September 28th, 2020. Only imagery with <40% cloud coverage was allowed, resulting in 10 potential multi-spectral images. Of those ten images only one contained enough visible shallow water to be suitable for this method of data processing. The process of finding suitable data is one of elimination and acceptance, when dealing with remote places like the poles – the data we have can only be so good, but it is better than nothing.

To understand how sparse ICESat-2 bathymetric photon returns are, a survey to parse out available bathymetric photon returns was conducted. The survey of potential datasets is confined to ICESat-2 ATL03 ground tracks which overpass the Canadian Archipelago from the -126.059˚ to -61.316˚ of longitude and was limited to data procured in August or September. Using Open Altimetry and manual inspection, the “Select a region” tool was used to draw bounding boxes

around areas where ground tracks crossed coastlines. The pop-up associated with the bounding box, ‘view elevation’ is utilized to scrub through ATL03 photon returns. If an area shows positive OSW returns, i.e., visible bathymetry returns and water surface returns classified as medium or high confidence, shown in Figure 3, it was recorded as an area where SDB mapping using ICESat-2 could be possible. The survey showed 495 ground tracks overpass the Northwest Territories and Nunavut, containing a total of 5422 total recorded datasets. To limit sea ice interference, only data collected in August or September were considered for this survey, dwindling the potential datasets to 681. Of those 681 datasets, only 116 ground tracks were found to contained at least one region showing bathymetric photon returns, therefore, about 2% of the ICESat-2 ATL03 ground tracks which cover the Canadian Arctic contain at least one region where bathymetric photon returns are present. While only 116 ground tracks contained bathymetric photon returns, 22 of those passes contained more than one location of bathymetry, therefore there are 138 location where bathymetric photon returns are available in the Canadian Archipelago. The process of identifying suitable data exposes the difficulty of conducting a SDB chart anywhere in the world, but specifically a complex polar environment where reliable LiDAR and multispectral data is sparse. Unfortunately, with a temporal resolution of only three years, the ICESat-2 LiDAR provides spotty coverage in OSW, making this method of mapping coastlines of the Arctic Ocean even more tedious. The limitation of suitable data will decrease as more data is procured; however, the outcomes of the data survey show that the likelihood of procuring bathymetric photon returns in the Canadian Arctic are slim.

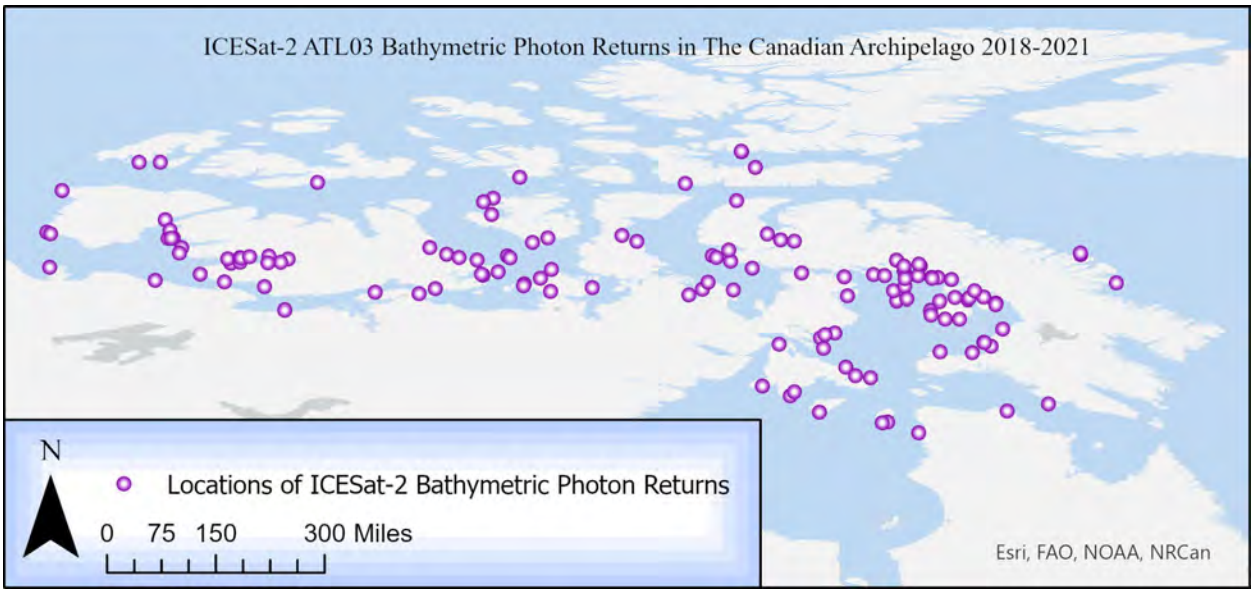

Figure 20: Locations where bathymetric photon returns were identified

Further work is needed into the applicability of these datasets, especially to conduct a multi-temporal analysis and understand if machine learning can be used to create a standard practice for data pre-processing. Considering the varying challenges of turbidity, tides, and atmospheric conditions, it would be difficult to conduct a uniform analysis across the Canadian Archipelago. Furthermore, alternative SDB approaches should be investigated to see if machine learning application or physics-based model can produce uniform models across large areas.

5.2. Atmospheric Correction

Atmospheric correction of multispectral imagery in complex climates such as the Arctic is best completed through SeaDAS, as tested through the performance analysis of four ocean color programs: SeaDAS, ACOLITE, Atmospheric and Radiometric Correction of Satellite Imagery (ARCSI), and Landsat 8 Surface Reflectance Code (LaSRC). Of the four programs, SeaDAS was shows to have the lowest root mean square error (RMSE) over complex waters and its errors are limited if imagery was taken when solar zenith is less than 76˚. (Ilori et al. 2019) While it is not required to have a solar zenith lower than 76˚, it is recommended to limit errors of

reflectance correction. Solar Zenith angle, the angle between a vertical position on the earth and the sun's rays, was calculated for a year between the latitudes of 60˚ and 90˚ at time steps of 1-minute shown in Figure 21. The color range is showing 0-100%: black to red probability of angle less than 80˚; therefore, days shown in other than red are more likely to produce imagery that is suitable for SDB.

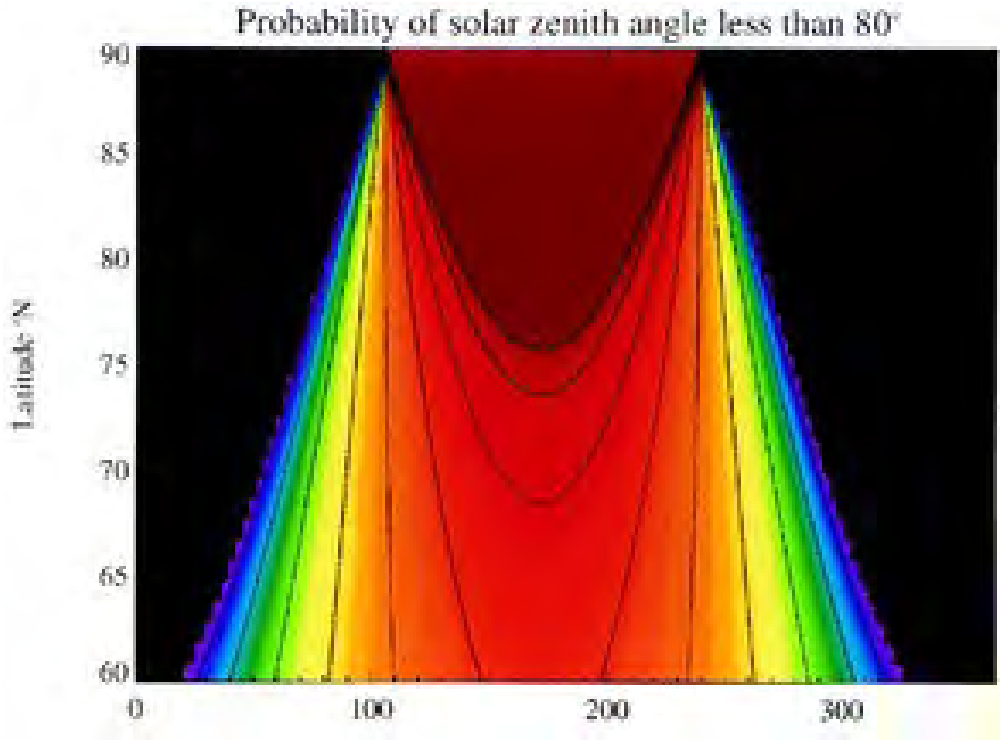

Figure 21: Average annual solar zenith from latitude 60˚ to 90˚ (Minnett 1999)

The time of year shown on the chart that experiences the greatest probability of having a solar zenith angle less than 80˚ is day 62 to 254 or March 2nd through September 10th. (Minnett 1999) Therefore, imagery taken in August and September have a decent probability of being procured when the solar zenith is less than 76˚, however there is no guarantee that the satellite passes over the area a time of day that exhibits solar zenith peaks. SeaDAS L2gen processing

uses geometry information such as solar zenith angle and viewing azimuth angle to incorporate geometry on a per-pixel basis. ACOLITE software does not process per-pixel geometry and instead uses the solar zenith angle and viewing azimuth angle found at the center of the scene. High-latitude regions can exhibit significant variation in solar zenith angle across a single OLI scene, therefore per-pixel reflectance is important to maintaining quality control and avoiding degradation of R_{rs} quality. For imagery in mid-latitude regions, ACOLITE R_{rs} processing is acceptable, but scenes located in polar regions should be processed with SeaDAS. (Pahlevan et al. 2017) While Babbel suggested the use of ACOLITE in their SDB workflow, it was ruled out as a viable software due to lack of reliability in high latitudes and the inability to mask land and cloud pixels. The masking of land, cloud, and other atmospherically inadequate pixels is automatically removed in SeaDAS's L2gen processing, making it more efficient than ACOLITE in both calculation of R_{rs} and atmospheric correction.

SeaDAS L2Gen processing was guided by Rodrigo Garcia, a member of the thesis committee residing over this work and an ocean science research fellow at the University of Western Australia, who provided a workflow to process Landsat-8 OLI/TIRS data through SeaDAS and L2gen, suggesting the output of R_{rs} data as a netCDF4 file. (Garcia 2021) Other export options in SeaDAS were explored but all other file extension options distort the original scale of the data. Once the netCDF4 file was imported into MATLAB, it maintained the correct WGS84 projection and R_{rs} scale however it was inverted to project upside down. To correct for this export error, the image was inverted in MATLAB to correctly project the individual reflectance raster images. When the netCDF4 file was opened with Python instead of MATLAB the inversion was not present. Since this issue could not be resolved with other export formats it was decided to invert the file in MATLAB to show the correct orientation of the image.

5.3. Refraction Correction

The refraction correction pioneered by Parrish et al. (2019) utilizes geometry to account for the change in speed of light that occurs to the LiDAR laser when it begins to travel through the water column instead of air and therefore the photons experience a change in the speed of light. Since the ICESat-2 satellite is not tuned to account for the change of substrate, refraction occurs to the specific bathymetric photon returns and therefore needs correction. The correction applies vertical and horizontal adjustments to account for the correct depth and position of the ATL03 photon. To ensure that the heights are correctly referenced before they undergo refraction correction, they are converted from ellipsoidal to orthometric heights. Datum transformations are inevitable in spatial analysis and the conversion from ellipsoidal to orthometric has proven to greatly affects the outcome of maximum and minimum bathymetric values. The tool suggested by Parrish was the NASA built program, in partnership with the National Geodedic Survey, Office of Coast Survey, and Center for Operational Oceanographic Products and Services, VDatum. The vertical datum transformation tool (VDatum) is a free software that runs on Java to perform transformations on geospatial data between varying vertical and horizontal datum systems. The VDatum transformations are fitted for American waterbodies and was suitable for the Caribbean St. Croix study area highlighted in Babel's work. It was found that most ATL03 points collected in the Bellot Strait that were initially identified as bathymetry when referenced to the WGS84/ITRF2014 became positive when converted to the EGM2008 geoid model. Once this was noticed other vertical projections were sought out. The Canadian Geodetic Vertical Datum of 2013 (CGVD2013) replaced the previous Canadian datum created in 1929 and is comparable with the other modern datums while representing mean sea level according to its best fit for the Canadian North American region. The confidence of the model is estimated to be 66%

with an accuracy of >0.03 m outside mountainous regions and above 0.1 m in areas with greater variation in terrain and topography. (Véronneau and Huang 2016) When converting the ATL03 photon heights to the CGVD2013, bathymetric points were retained. To compare the effects of the datum transformation, Table 7 compares the maximum and minimum height values associated with each orthometric conversion type. Max and Min values reflect bathymetric data after reflectance correction and manual point filtering to isolate bathymetry.

Table 8: Max and Min H values based on Datum Projection

Orthometric Conversion Type	**Max H value**	**Min H value**
ITRF2014 (Ellipsoidal)	0.00007	-15.284
EGM2008 (Orthometric) [Vdatum]	9.9997	0.7317
CGVD2013 (Orthometric) [GPS-H]	0.00007	-28.049

Refraction correction is applied through MATLAB following the equations defined by Parrish et al. (2019) but reorganized for clarity of variables. The model takes parameters such as solar azimuth and elevation to fit the refraction correction directly from the ATL03 HDF5 data file from NSIDC. For this reason, bulk processing of ICESat-2 tracks is not possible and individual variables for each track must be calculated. For this survey, the mean of ref_elev and ref_azi were used in equation 2 and the variable k, respectively. The other variables needed are the refractive indices of air (n_1=1.00029) and water (n_2= 1.343) were adopted from Parrish et al. (2019).

5.4. Collocation

After the ATLO3 has undergone orthometric datum conversion and refraction correction, the H_{LiDAR} image is combined with reflectance layers R_{rs} (443 nm), R_{rs} (482 nm), R_{rs} (561 nm) to

collocate the height values to a raster pixel which contains a reflectance value. The GIS adage 'garbage in, garbage out' is a strong reminder of the data processing step to remove outliers. When refraction corrected points deeper than 23 m was included, the collocation and multiband fit returned statistically insignificant data. Collocation was conducted using various buffers for the training data, but the model returned the lowest MSE when training bathymetric points were constricted to depths between 0 m and 23 m. The collocation process took the longest of all the models, matching each raster pixel to a subset of H_{LiDAR} data and accepting the orthometric mean value of H found in each pixel to generate training data for the empirical models. The collocation model returned 811 raster pixels that contained both bathymetry and reflectance from a total of 390,140 H points collected from the ATL03 which contained bathymetry. While alternative collocation methods were not explored in this thesis, it was suggested by Rodrigo Garcia during the defense of this methodology that the collocation could be improved upon by using an alternative algorithm to estimate average depth in each raster cell. When comparing thousands of LiDAR points contained in a 30 m x 30 m Landsat 8 Raster cell, there could be a more accurate way of representing average water depth than using only the mean orthometric height. In future work, alternative programs outside of MATLAB or using alternative scripts should be considered, as well as the efficiency, accuracy, and approach of collocation methods should be tested further.

5.5. SDB Empirical Algorithm Fits

Two different empirical algorithms were used in this thesis to test efficiency of using reflectance from different bands to calculate depth. The results were processed through linear regression in attempts to understand the best fit for the model. It was shown early on during multiband value algorithm processing that the red band, R_{rs}(655 nm) resulted in MATLAB errors

reporting that the matrix Jacobian was singular and therefore the data was too low quality and would not produce statistically significant results. Considering several studies mentioned that reflectance in the red and near infrared regions were unreliable, it was decided to omit R_{rs} (655 nm) from the MBVA. The results of the MBVA were better than the TBVA, shown through the following measures of confidence: root mean square error (RMSE), r^2 value, and P value reported by each empirical algorithm. The TBVA contained RMSE of 2.38 m, an r^2 value of 0.675, and a P value of 0.00659. The MBVA contained a RMSE of 1.16, an r^2 value of 0.945, and a P value of 0.00139. The error analysis shows that the MBVA has far greater linear association than the TBVA, meaning the inclusion of the coastal aerosol band (R_{rs} 443 nm) contributed significantly to the positive liner fit. If an r^2 value of 1.0 is equivalent to 100% predictability or certainty, the MBVA can be inferred to have 94.5% certainty that the model returned bathymetric data that can be considered statistically significant, while the TBVA only returned a data with 67.5% certainty. Another indicator of statistical improbability is that P values for both algorithms are less than 0.05, the recommended P value for significance, reflecting on the reliability of the model across the study area. Both models pass this threshold and can be considered significant, however the MBVA did have a greater fit than the TBVA.

Table 9: Multiband Value Algorithm Linear Regression Coefficients

Estimated Coefficients	Estimate	Standard Error	tStat	P value
α_0	534.71	200.49	2.667	0.044509
α_1	255.01	46.594	4.8291	0.0047603

α_3	-101.11	66.87	-1.512	0.19093
α_4	-12.467	19.465	-0.64048	0.55006

The MBVA total P value = 0.00139, which is a great indicator of statistical certainty. The r^2 = 0.945 meaning there is a large positive linear association (94.5%) between the linear regression of H_{LiDAR} and H_{imger}.

Table 10: Two Band Value Algorithm Linear Regression Coefficients

Estimated Coefficients	Estimate	Standard Error	tStat	P value
α_0	508.15	138.59	3.6666	0.0080005
α_1	-10.884030	2.513322	-4.330535	1.603679

The TBVA P value = 0.00659, while still an indicator of statistical certainty, is much higher than the P value for the MBVA, meaning that it has a worse fit.

Chapter 6 Conclusion

The motivation behind this thesis began as desire to map change in coastlines, or better, understand the tools available to cartographers that help represent the border between land and ocean. It is with the pursuit of creating an accurate model of Arctic shoreline in mind that the rabbit hole of satellite derived bathymetry was followed. The process, at its most general, is creating an index between ocean color reflectance and LiDAR derived depths to interpolate bathymetry across a surface of observable shallow water. In practice, this method is a complex series of atmospheric, geodetic, and geometric corrections combined to generalize the ocean sub-surface. What became most clear after completing the methods described in this thesis is that SDB models are best when localized and at this time cannot be reproduced across a large area such as the Canadian Archipelago.

As of 2021, we do not have great bathymetric charting of coastlines in the Canadian Archipelago. While procuring bathymetry through satellite remote sensing is possible, the scarcity of locations that have suitable data to perform SDB leads me to believe that this method would only produce minimal bathymetry across the Canadian Archipelago. Due to the variations in bottom substrate, turbidity, tides, and data collection time, at this time, a standardized index of depth as it relates to OSW in the Arctic cannot be completed. The hypothesis states that SDB in the Bellot Strait can be accomplished with reasonable statistical certainty and similar methods can be utilized to map regions with comparable data across the Canadian Archipelago. It was found that in the case of the Bellot Strait that the MBVA has a 27% higher certainty of modeling bathymetry correctly than the TBVA, however both models offer a bathymetric interpolation with acceptable statistical certainty. Upon further inspection of the available ground tracks, there

are currently 138 locations that contain bathymetric photon returns in the Canadian Archipelago. Greater investigation is needed to determine if these datasets have accompanying multispectral imagery taken with a solar zenith less than 80˚ and with cloud coverage <40%. Since the multiband and band ratio SDB approaches are heavily influenced by the conditions of the data collection, the quality of SDB derived from this data cannot be assessed until further ground truth research is conducted.

It is with those 138 locations of bathymetric photon returns in mind that I recommend the Seabed 2030 project, IBCAO, and GEBCAO all consider using the refraction correction generated by Parrish to obtain LiDAR corrected depths to use in the greater interpolation of Arctic Ocean bathymetric models. The bathymetric photon returns extend anywhere from 10 meters to 2 miles and each location contains its own range of maximum depth, however most datasets showed at least 15 m of bathymetry. By only using the ICESat-2 LiDAR heights, uncertainties associated with the Landsat 8 OLI could be omitted and either higher resolution multispectral data or another interpolation method could be leveraged. Considering that both the IBCAO and the GEBCAO use data from a wide variety of sensors, LiDAR bathymetry from ICESat-2 satellites would be compatible however the orthometric points in CGVD2013 would need to be converted to polar stereographic projection. Most of the datasets used in these conglomerates come from multibeam sonar that would not record depths in OSW, therefore ICESat-2 bathymetry could help reduce uncertainties of the interpolation of NSB.

The NSIDC processes 21 separate datasets to optimize a variety of parameters, mostly related to terrain elevation, glacial and sea ice height, cloud properties, sea surface height, and aerosol fraction. (NSIDC 2021) Through the use of the refraction correction applied in this thesis, bathymetric photon returns could be optimized as a data product on OpenAltimetry.

The conclusion of this process is that data acquisition is complex and precocious, and models are highly dependent on atmospheric conditions, but when the data is preprocessed correctly, statistically conclusive bathymetric models can be achieved. Further study is required to understand how multi-temporal analysis can be used to generate a greater acquisition of reflectance data to feed into the collocation model. There is still a large amount of work to be done before SDB charts will be accepted as navigational resources, however this process is being discussed widely across the hydrographic and data science community and great progress in this field has been made since the launch of ICEsat-2. It will be interesting to share this work with groups such as DFO, CHS, NOAA, IHO, IBCAO and the Seabed 2030 project to see how the method in this thesis could contribute to data of various Arctic databases and bathymetric models. Further development of conversions for Arctic orthometric projections are needed as many of these tools, such as Vdatum or ACOLITE, are not built for northern latitudes. This thesis shows that band ratio and multiband value SDB methods are both possible in the Bellot Strait however the MBVA was more statistically significant than the TBVA. Further investigation into the use of these models on remaining areas of the Canadian Archipelago where data is available need to be monitored. There is great potential for SDB in the Arctic using satellite remote sensing, greater modeling is needed as we procure more ICESat-2 data and as ice-free shoreline in the Arctic continues to increase annually.

References

Ackerman, E. 2017. “When Lasers Took to the Air to Measure the Earth” History of Technology. IEEE Spectrum. Available at: < https://spectrum.ieee.org/when-lasers-took-to-the-air-to-measure-the-earth > Accessed July 29, 2021

Ahola, Ryan, et al. 2018 "Satellite derived bathymetry for Arctic charting: a review of sensors and techniques for operational implementation within the Canadian Hydrographic Service." SPIE.

ArcticNet. n.d. “Vision and Mission” About Us. ArcticNet INC. Available at: <https://arcticnet.ulaval.ca/vision-and-mission/about-us >

Babbel, B. J., Parrish, C. E., & Magruder, L. A. 2021. “ICESat-2 elevation retrievals in support of satellite derived bathymetry for global science applications.” Geophysical Research Letters, 48, e2020GL090629.

Bailey, S., Franz, B., Werdell, J. 2010. “Estimation of near-infrared water-leaving reflectance for satellite ocean color data processing.” Optical Society of America

Bour, W., Loubersac, L., Rual, P. 1986. “Thematic mapping of reeds by processing of simulated SPOT satellite data: application to the Tronchus niloticus biotope on Tetembia Reef (New Caledonia)” *Marine Ecology Progress Series.*

Canadian Hydrographic Service. 2020. *CHS Chart 7552: Bellot Strait and Approaches*. Captains Nautical.

Chénier, R., Faucher, M., and Ahola, R. 2018. "Satellite-Derived Bathymetry for Improving Canadian Hydrographic Service Charts." *ISPRS International Journal of Geo-Information.*

Committee, IASC. 2020 “IASC Organization.” International Arctic Science Committee, Accessed December 1, 2021, Available at: <https://iasc.info/about/organisation>.

Coveney, S., Monteys, X., Kelleher, B., Hedley, J. 2020 “Bathymetric Extraction from ICESat-2 Advanced Topographic Laser Altimeter System Photon returns: Depth penetration in diverse geophysical contexts” *European Geosciences Union 2020 Conference EU-Intertide*

Government of Canada. 2016 “Nautical Charts and Services” Fisheries and Oceans Canada.” Accessed July 5, 2021. Available at: < https://www.charts.gc.ca/index-eng.html>

Government of Canada, Fisheries and Oceans (DFO). 2021 “Bellot Strait East Tides, Currents, and Water Levels.” 2020 Tide Tables. Accessed July 16, 2021. https://www.waterlevels.gc.ca/eng/data/table/2020/wlev_sec/5917

Ilori, C., Pahlevan, N., Knudby, A. 2019. "Analyzing Performances of Different Atmospheric Correction Techniques for Landsat 8: Application for Coastal Remote Sensing" Remote Sensing 11, no. 4: 469.

International Hydrographic Organization. 2021. “About the IHO” IHO. Last modified January 14, 2021. Available at: <https://iho.int/en/about-the-iho>

IOC-UNESCO. n.d. “Intergovernmental Oceanographic Commission” UNESCO. Accessed July 5, 2021. Available at: <https://ioc.unesco.org/>

Jakobsson, M., Mayer, L., Monahan, D. 2014. “Arctic Ocean Bathymetry: A Necessary Geospatial Framework.” The Arctic Observing Summit. *Arctic Institute of North America.*

Jakobsson, M. and Mayer, L., 2019. “Evolving Arctic Bathymetry: The International Bathymetric Chart of the Arctic Ocean (IBCAO) Version 4.0 Compiled Under the Auspices of the Nippon Foundation-GEBCO-Seabed 2030 Project.” The Center for Coastal and Ocean Mapping. Available at: <http://ccom.unh.edu/publications/evolving-arctic-bathymetry-international-bathymetric-chart-arctic-ocean-ibcao-version> [Accessed 3 December 2021].

Jakobsson, M., et al. 2020. “The International Bathymetric Chart of the Arctic Ocean Version 4.0. Vol. 7” Springer Science and Business Media LLC.

Jupp, D., Mayo, K., Kuchler, D., Claasen, D., Kenchington, R., Guerin, P.1985. “Remote sensing for planning and managing the great barrier reef of Australia” *Photogrammetria.*

Khalsa, S.J.S., Borsa, A., Nandigam, V. et al. 2020. “Rapid analysis and visualization of Spaceborne altimeter data.” *Earth Sci Inform* OpenAltimetry,com Accessed October 2021

Knudby, A., Newman, C., Shaghude, Y., Muhando, C. 2010. “Simple and effective monitoring of historic changes in nearshore environments using the free archive of Landsat imagery” *International Journal of Applied Earth Observation and Geoinformation.*

Kutser, T., Headly, J., Giardino, C., Roelfsema, C., Brando, V., 2020 "Remote Sensing of Shallow Waters – A 50 year Retrospective and Future Directions." *Remote Sensing of Environment*.

Landsat Mission. 2021. “Landsat Collection 1 vs Collection 2 Summary.” Landsat Collection 1 vs Collection 2 Summary | U.S. Geological Survey, April 30, 2021. https://www.usgs.gov/media/files/landsat-collection-1-vs-collection-2-summary.

Landsat 8 OLI/TIRS. Landsat 8 Level 1 Collection 1. “Image ID: LC08L1TP_040009_20200914_01_T1” Geotiff Data Product. EarthExplorer. USGS. September 14, 2020.

Lee, Z., Carder, K., Mobley, C., Steward, R., Patch, J., 1999 "Hyperspectral remote sensing for shallow waters: 2. Deriving bottom depths and water properties by optimization," *Applied Optics.*

Lee, Z., Shangguan, M. Garcia, R. Lai, W., Lu, X., Wang, J., Yan, X., 2021 "Confidence Measure of the Shallow-Water Bathymetry Map obtained through the Fusion of LiDAR and Multiband Image Data." *Journal of Remote Sensing*.

Levere, T. 1988. "Vilhjalmur Stefansson, the Continental Shelf, and a New Arctic Continent" Cambridge University Press. *The British Society for the History of Science*.

Liu, X., Ma, L., Wang, J., Wang, Y., Wang, L. 2017. "Navigable windows of the Northwest Passage." *Polar Science.*

Lyzenga, D. 1981. "Remote Sensing of bottom reflectance and water attenuation parameters in shallow water using aircraft and Landsat data" International Journal of Remote Sensing.

Lyzenga, D. 1985. "Shallow-water bathymetry using combined LiDAR and passive multispectral scanner data." *null* 6, no. 1: 115-125.

McKinna, L., Werdell, J. 2018. "Approach for identifying optically shallow pixels when processing ocean-color imagery" *Optics Express.*

Minnett, P. 1999. " The Influence of Solar Zenith Angle and Cloud Type on Cloud Radiative Forcing at the Surface in the Arctic" *Journal of Climate.*

Mumby, P., Baker, M., Raines, P., Ridley, J., Phillips, A. 1994 "The Potential of Spot Panchromatic Imagery as a Tool for Mapping Coral Reefs" *Environmental Research Institute Michigan.*

NASA EARTHDATA. n.d. "Earthdata Search" Accessed July 16, 2021. https://search.earthdata.nasa.gov/search

National Snow and Ice Data Center. 2021. "ATLAS/ICESat-2 L2A Global Geolocated Photon Data, Version 4" Accessed July 16, 2021. https://nsidc.org/data/ATL03

Neumann, T. A., A. Brenner, D. Hancock, J. Robbins, S. et. AL. 2019. ATLAS/ICESat-2 L2A Global Geolocated Photon Data, Version 1. "Segment ID 400641 2020-08-12". Boulder, Colorado USA. *NSIDC: National Snow and Ice Data Center.*

Nikishin, A., et al. 2021. "Arctic Ocean Mega Project: Paper 1 - Data Collection." *Earth-Science Reviews*

NOAA. 2021. "About our agency" National Oceanic and Atmospheric Administration. U.S. Department of Commerce. Last Modified May 25, 2021. https://www.noaa.gov/about-our-agency

NOAA. 2021. “What is sonar?” National Oceanic and Atmospheric Administration. U.S. Department of Commerce. Last Modified February, 26, 2021. https://oceanservice.noaa.gov/facts/sonar.html

NOAA/NCEI & World Data Service for Geophysics. 2012. “IBCAO.” International Bathymetric Chart of the Arctic Ocean. https://www.ngdc.noaa.gov/mgg/bathymetry/arctic/arctic.html.

NRCan, Natural Resources Canada. 2020 “Confirm the Accuracy of the Heights and Stability ... - NRCAN.” Height Reference System Modernization. Federal Government of Canada.

Olmanson, L., Bauer, M., Brezonik, P. 2008. “A 20-year Landsat water clarity census of Minnesota’s 10,000 lakes” *Remote Sensing of Environment.*

Pahlevan, N, J R. Schott, and B A. Franz. 2017 “Landsat 8 Remote Sensing Reflectance (R_{rs}) Products: Evaluations, Intercomparisons, and Enhancements.” Remote Sensing of Environment 190 289–301.

PAME. 2021. “Protection of the Arctic Marine Environment.” Organization Working Groups. Accessed July 5, 2021. https://arctic-council.org/en/about/working-groups/pame/

PAME. 2021. “Compendium of Arctic Ship Accidents” Projects. Arctic Council. Accessed on July 5, 2021. https://www.pame.is/projects-new/arctic-shipping/pame-shipping-highlights/457-compendium-of-arctic-ship-accidents

Parrish, C., Magruder, L., Neuenschwander, A., Forfinski-Sarkozi, N., Alonzo, M., Jasinski, M. 2019. "Validation of ICESat-2 ATLAS Bathymetry and Analysis of ATLAS’s Bathymetric Mapping Performance" Remote Sensing 11, no. 14: 1634.

Pawlowicz, R. “T_Tide MATLAB” University of British Columbia, March 2011 Accessed July 16, 2021. https://www.eoas.ubc.ca/~rich/

Pe'eri, S., et al. 2015. “Reconnaissance surveying of Bechevin Bay, AK using satellite-derived bathymetry.” UNH Center for Coastal and Ocean Mapping.

Polyak, L. and Martin J. 2011. Quaternary Sedimentation in the Arctic Ocean: Recent Advances and further Challenges. The Oceanography Society

Ranndal, H.; Sigaard Christiansen, P.; Kliving, Et. AL. 2021. “Evaluation of a Statistical Approach for Extracting Shallow Water Bathymetry” Signals from ICESat-2 ATL03 Photon Data. Remote Sens. 2021, 13, 3548.

RBINS. “ACOLITE: Generic Atmospheric Correction Module.” GitHub. Royal Belgian Institute of Natural Sciences, April 21, 2021. https://github.com/acolite/acolite.

Smith, V., Rogers, R., Reed, L. 1975. “Automated mapping and inventory of Great Barrier Reef zonation with Landsat data” *Institute of Electrical and Electronics Engineers.*

Stumpf, R., Holderied, K., Sinclair, M. 2003. “Determination of water depth with high-resolution satellite imagery over variable bottom types,” Association for the sciences of Limnology and Oceanography.

United States Geological Survey. n.d. “EarthExplorer” Accessed July 16, 2021. https://earthexplorer.usgs.gov/

Véronneau, M, and J Huang. 2016. “The Canadian Geodetic Vertical Datum of 2013 (CGVD2013).” GEOMATICA 70, no. 1 9–19.
Weber, J. 1983. “Maps of the Arctic Basin Sea Floor: A History of Bathymetry and Its Interpretation” Arctic Vol. 36. *Arctic Institute of North America*.

Wulder, M., Loveland T., Roy, D., Crawford, C. et AL. 2019 "Current status of Landsat program, science, and applications, Remote Sensing of Environment, Volume 225.

Zhang, J.-Y., Zhang, J., Ma, Y., Chen, A.-N., Cheng, J., and Wan, J.-X. 2019. “Satellite-derived bathymetry model in the Arctic waters based on support vector regression.” Advances in Remote Sensing and Geoscience Information Systems of Coastal Environments. Journal of Coastal Research.

Appendix A

IBRU

Durham University
Department of Geography

Maritime jurisdiction and boundaries in the Arctic region

- Canada territorial sea and exclusive economic zone (EEZ)
- Canada continental shelf beyond 200 M (see note 2)
- Denmark territorial sea and EEZ
- Denmark continental shelf beyond 200 M (note 3)
- Iceland territorial sea and EEZ
- Iceland continental shelf beyond 200 M (note 3)
- Norway territorial sea and EEZ / Fishery zone (Jan Mayen) / Fishery protection zone (Svalbard)
- Norway continental shelf beyond 200 M (note 4)
- Russia territorial sea and EEZ
- Russia continental shelf beyond 200 M (note 5)
- Norway-Russia Special Area (note 6)
- USA territorial sea and EEZ
- Potential USA continental shelf beyond 200 M (note 7)
- Overlapping Canada / USA EEZ and territorial sea (note 8)
- Russia-USA Eastern Special Area (note 9)
- Seabed beyond any state's continental shelf (note 1)
- Straight baselines
- Agreed boundary
- Median line
- Svalbard treaty area (note 10)
- Iceland-Norway joint zone (note 11)
- Main 'Northwest Passage' shipping routes through Canada claimed internal waters (note 12)
- Internal waters
- Land
- North Pole

For an explanation of continental shelf submissions and other zones depicted on this map, please see briefing notes at
https://www.durham.ac.uk/research/institutes-and-centres/ibru-borders-research/maps-and-publications/maps/arctic-maps-series/

Appendix B

MATLAB Code to perform refraction correction, collocation, MBVA, and TBVA.

Refraction Correction:

```
clear variables; close all; clc

%Extract strong ground tracks and run them through conversion from
%ellipsoid to orthometric data. The tool GPS-H from the Canadian
%Hydrographic Survey was used in this code however it is recommended to
%convert the data to the orthometric model which best fits your study
%area.

LOC = [csvread('GPS_H\GT1L_Ortho.csv',1,0); ...
       csvread('GPS_H\GTL2_Ortho.csv',1,0); ...
       csvread('GPS_H\GTL3_Ortho.csv',1,0) ];
azi = -2.122217210653705; %This is average of ref_azi from the h5 file
elev = 1.563192527542595; %average ref_elev from hf ICESat-2 ATL03 file

% A little less storage-efficient, but MUCH more readable (You who dare
repeat this process).
lat = LOC(:,1);
lon = LOC(:,2);
h = LOC(:,3);

theta1 = pi/2 - elev;
kappa = azi;
n1 = 1.00029;    %n1 and n2 are the refractive indices of air and water
n2 = 1.343;

theta2 = asin( n1*sin(theta1) / n2 );
S = h / cos(theta1);
R = S*n1/n2;
gamma = pi/2 - theta1;
P = sqrt( R.^2 + S.^2 - 2*R.*S*cos(theta1-theta2) );
alpha = asin( R*sin( theta1-theta2 ) ./ P);
beta = gamma - alpha;

horzoff = P.*cos(beta); % delta Y in the paper
vertoff = P.*sin(beta); % delta Z in the paper

latoff = horzoff*cos(kappa); % delta N in the paper
lonoff = horzoff*sin(kappa); % delta E in the paper

lat = lat + latoff;
lon = lon + lonoff;
h = h + vertoff;

writematrix([lat lon h],'refcorr.txt');
fprintf('Done :)\n');
```

Collocation:

```
clear variables; close all; clc

LOC = readmatrix('refcorr.txt');
idx = LOC(:,3) > 0;
LOC(idx,:) = [];
idx = LOC(:,3) < -23;
LOC(idx,:) = [];

Info = ncinfo('2020_14_09.nc');% .nc file from SeaDAS
ncfile = Info.Filename;
lats = ncread(ncfile,'lat');
lons = ncread(ncfile,'lon');
lats = lats';
lons = lons';

Rrs443 = ncread(ncfile,'Rrs_443');
Rrs482 = ncread(ncfile,'Rrs_482');
Rrs561 = ncread(ncfile,'Rrs_561');
Rrs655 = ncread(ncfile,'Rrs_655');
Rrs443 = Rrs443';
Rrs482 = Rrs482';
Rrs561 = Rrs561';
Rrs655 = Rrs655';

min443 = 0.0023233603215;
max443 = 0.0136837861662;
min482 = 0.002054844596;
max482 = 0.0117353758214;
min561 = 0.000186953921;
max561 = 0.0051008600112;
min655 = -0.0004717842139;
max655 = 0.0014484306939;

% Rescaling reflectances based on Seadas info (true data shift)

a = min(Rrs443,[],'all');
b = max(Rrs443,[],'all');
Rrs443 = min443 + (Rrs443-a)/(b-a)*(max443-min443);
a = min(Rrs482,[],'all');
b = max(Rrs482,[],'all');
Rrs482 = min482 + (Rrs482-a)/(b-a)*(max482-min482);
a = min(Rrs561,[],'all');
b = max(Rrs561,[],'all');
Rrs561 = min561 + (Rrs561-a)/(b-a)*(max561-min561);
a = min(Rrs655,[],'all');
b = max(Rrs655,[],'all');
Rrs655 = min655 + (Rrs655-a)/(b-a)*(max655-min655);

%throw out the MANY MANY nans >:/
```

```
% idx = isnan(Rrs443);
% lats(idx) = [];
% lons(idx) = [];
% Rrs443(idx) = [];
% Rrs482(idx) = [];
% Rrs561(idx) = [];
% Rrs655(idx) = [];

fprintf('Loaded and processed reflectance data.\n');
```

Multiband Value Algorithm and Two Band Value Algorithm:

```
clear variables; close all; clc
LOC = readmatrix('collocatedRrsHeights.txt');
%[ lat lon h Rrs443 Rrs482 Rrs561 Rrs655 ]

Info = ncinfo('2020_14_09.nc');
ncfile = Info.Filename;
lats = ncread(ncfile,'lat');
lons = ncread(ncfile,'lon');
Rrs443 = ncread(ncfile,'Rrs_443');
Rrs482 = ncread(ncfile,'Rrs_482');
Rrs561 = ncread(ncfile,'Rrs_561');
Rrs655 = ncread(ncfile,'Rrs_655');
Rrs443 = Rrs443';
Rrs482 = Rrs482';
Rrs561 = Rrs561';
Rrs655 = Rrs655';

min443 = 0.0023233603215;
max443 = 0.0136837861662;
min482 = 0.002054844596;
max482 = 0.0117353758214;
min561 = 0.000186953921;
max561 = 0.0051008600112;
min655 = -0.0004717842139;
max655 = 0.0014484306939;

% Rescaling reflectances based on Seadas info (true data shift)

a = min(Rrs443,[],'all');
b = max(Rrs443,[],'all');
Rrs443 = min443 + (Rrs443-a)/(b-a)*(max443-min443);
a = min(Rrs482,[],'all');
b = max(Rrs482,[],'all');
Rrs482 = min482 + (Rrs482-a)/(b-a)*(max482-min482);
a = min(Rrs561,[],'all');
b = max(Rrs561,[],'all');
Rrs561 = min561 + (Rrs561-a)/(b-a)*(max561-min561);
a = min(Rrs655,[],'all');
b = max(Rrs655,[],'all');
Rrs655 = min655 + (Rrs655-a)/(b-a)*(max655-min655);
```

```
fprintf('Loaded, rescaled reflectance values.\n');

% % % 3 BAND MULTIBAND – after omitting Rrs 655.
LOC3band = LOC(:,3:6);
h = readmatrix('collocatedRrsHeights.txt');
rs = size(Rrs443);
LOC3band = [reshape(h,prod(rs),1), reshape(Rrs443,prod(rs),1),...
            reshape(Rrs482,prod(rs),1), reshape(Rrs561,prod(rs),1)];
fun = @(alpha, R) alpha(1) + alpha(2)*log(R(:,1)) +
alpha(3)*log(R(:,2))...
                        + alpha(4)*log(R(:,3));
[beta, resid, J, covb, mse] = nlinfit( LOC3band(:,2:4), LOC3band(:,1),...
                                       fun, [1 1 1 1]);

% % % 2 BAND FIT - using just 482 and 561.
LOC2band = LOC(:,[3 5 6]);
LOC2band = [reshape(h,prod(rs),1), ...
            reshape(Rrs482,prod(rs),1), reshape(Rrs561,prod(rs),1)];

fun = @(alpha, R) alpha(1) + alpha(2)* log(R(:,1))./log(R(:,2));
[beta, resid, J, covb, mse] = nlinfit(LOC2band(:,2:3), LOC2band(:,1),...
                                       fun, [1 1]);
```